NMR Multiple Quantum Filters via RF Gradients
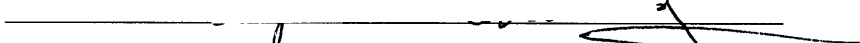
by

Cynthia Fu-Yu Chuang

B.S. Electrical Engineering, M.I.T., 1990
M.S. Bioengineering, University of Pennsylvania, 1992

SUBMITTED TO THE DEPARTMENT OF
NUCLEAR ENGINEERING
IN PARTIAL FULFILLMENT OF THE
REQUIREMENTS FOR THE
DEGREE OF
MASTER OF SCIENCE IN NUCLEAR ENGINEERING
at the
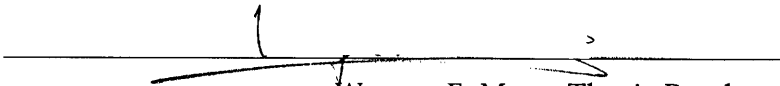MASSACHUSETTS INSTITUTE OF TECHNOLOGY
May 1994

© Massachusetts Institute of Technology
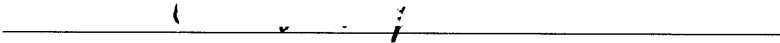
Signature of Author: _____
Department of Nuclear Engineering, May 18, 1994

Certified by: _____
David G. Cory, Thesis Supervisor
Assistant Professor, Department of Nuclear Engineering

_____
Werner E. Maas, Thesis Reader
Bruker Instruments, Inc., Billerica, MA

Accepted by: _____
Allan Henry, Chairman
Departmental Committee on Graduate Students

NMR Multiple Quantum Filters via RF Gradients

by

Cynthia Fu-Yu Chuang

Submitted to the Department of Nuclear Engineering
on May 18, 1994 in partial fulfillment of the
requirements for the Degree of
Master of Science in Nuclear Engineering

ABSTRACT

The goal of this research was to design and test multiple quantum filters using RF gradients. The POMA program was used to simulate the pulse sequence which were developed to select a desired multiple quantum filter coherence pathway. Multiple quantum filter pulse sequences were then implemented on a Bruker AC-400 spectrometer to test the effectiveness of the RF gradient method, and 2-D COSY experiments were performed to demonstrate the coherence transfer pathway and spin connectivities. It was found that multiple quantum filters can be successfully implemented using RF gradients.

Thesis Advisor: David G. Cory
Assistant Professor, Department of Nuclear Engineering

Acknowledgement

It would be difficult for me to express my gratitude to Professor David G. Cory for his patience, his continual support, guidance and encouragement. I would not have successfully completed this work without his support, and I definitely learned a lot while learning to do research with him. Thanks a lot, Professor Cory!

I would like to thank Werner E. Maas, Ph.D. for his patience in explaining the multiple quantum filter concepts, his help in solving some of the problems I encountered while conducting experiments, and his assistance in reading and critiquing my thesis.

I would also like to thank everybody in the lab for making the lab a happy place. I especially thank Yang Zhang for his help on related topics for my research, and his support for the difficult times I had with the theory and the experiments. Yuan Cheng and Wurong Zhang helped me a lot with problems concerning the physics of NMR, thanks a lot, guys. I would also like to thank Sungmin Choi and Chris Drew for being very friendly and helpful in the lab. Of course, I would have to thank John Zhang for bringing in the candies, in addition to his help on the subject of NMR. The candies gave me something to munch on when I was nervous and under pressure.

I truly thank my parents and my grandmother for their unconditional love and support, without them, I don't think I could have finished these two years here at M.I.T.. I would like to especially thank my sister Sandy for her love, support and understanding in listening to my complaints throughout the years. Sandy, I really appreciate it. It is to my family that this thesis is gratefully dedicated.

Cynthia Fu-Yu Chuang, 18 May 1994

Contents

List of Figures

List of Tables

Chapter I

Introduction

1.1 Overview

Proteins and nucleic acids are the fundamental building blocks of our bodies. The study of the structural details of these large complex molecules therefore is a central theme in biomedical research. Nuclear Magnetic Resonance (NMR) provides an excellent tool for structure elucidation[9,12]. From NMR's ability to establish bonding connectivity and through-space proximity of nuclei [8,9,12], it provides a widely used approach for the elucidation of spatial conformation of large molecules, such as the secondary, tertiary and quaternary structures of proteins. In 2-D NMR, COSY (COrrelation SpectroscopY) experiments [6,8] are used to explore J-coupling interactions, and NOESY (Nuclear Overhauser Enhancement SpectroscopY) experiments [6,8] are used to demonstrate dipolar interactions. With these experiments, the proximity between coupled proton spins can be determined, the number of equivalent protons can be measured from the signal intensity, and the number of adjacent protons can be determined from the multiplets. Therefore, multi-dimensional COSY and NOESY experiments are fundamental in the determination of sequence and spatial conformation of large biomolecules.

Since the structure of large biomolecules is extremely complex, the corresponding NMR spectrum usually consists of many resonances, some of which overlap with one another. The determination of each resonance frequency and the relationship it has with other protons of the same molecule are extremely difficult. In addition, the solvent signal is usually many times

larger than that of the biomolecule under study, and the biomolecule's resonance signals are usually obscured. Therefore, a common practice in the determination of molecular structure in high-resolution NMR is to filter out unwanted spin responses. An example is multiple quantum filtering, which suppresses all signals except those that arise from coherence transformations that pass through a very specific multiple quantum state. Since only coupled spin can have states with quantum number of more than 1, and since multiple quantum states can only be achieved by applying certain pulse trains, it is possible to suppress all uncoupled spins and unwanted quantum states. Since the signals observed in multi-pulse NMR experiments are superpositions of different quantum state components following different "coherence-transfer pathways" during the course of the pulse sequence, by performing a pulse sequence that specifically selects a particular coherence-transfer pathway, all signals from other pathways are dephased and are not observed[6]. Traditionally, this selectivity is achieved by phase cycling. Since the selectivity is built up piece by piece, phase cycling inherently requires many scans to average out the undesired coherence pathway, and may lead to an inefficient use of spectrometer time[4]. This inefficiency may be even more pronounced in multidimensional experiments. The phase cycling method also has limited dynamic range since the spectrometer's A-to-D converter has to digitize the unwanted signal as well as the desired signal throughout the whole experiment.

To efficiently utilize the spectrometer time, gradient methods have been suggested as an alternative to phase cycling[1,5]. The use of B_0 field gradient poses some technical difficulties, such as eddy currents and B_0 shifts. Since

these problems can be avoided by applying a Radio Frequency (RF) gradient, there has been growing interest in using RF gradients for coherence-pathway selection[4,10].

RF gradient methods provide important pathway selection schemes with as little as one scan of the experiment. They can suppress the solvent resonance, reduce spectral artifacts, and restrict the range of observed coherence pathway transformations[4,10].

In this work, RF gradient experiments were created based on the experiment symmetry and intuition. These were then simulated via a known Product Operator Formalism *Mathematica* program (POMA)[7], to verify the desired experiment properties. In particular, the sensitivity to various multiplet structures were investigated. Then the pulse sequence was translated into an automation program and implemented on the NMR spectrometer. 1-D experiments were performed to verify the validity of the multiple quantum filter pulse sequences. Then 2-D experiments were performed to explore the robustness of the method.

1.2 Background

A major concern for NMR researchers is the suppression of solvent resonance peak since its intensity is often much larger than the peak intensities of the compound under study. Often times, with very complex spectra, to increase the dynamic range of the A-to-D converter and to simplify the spectra, it is also desirable to suppress other coupled spins[9,12], multiple quantum filters will suppress these unwanted spins and leave only the desired

spins. A multiple quantum filter of order p eliminates the responses of all spin systems with $N < p$ coupled nuclei and can be thought of as a high-pass filter[6]. The filtering process is usually achieved by the following steps: 1) converting the spins into a suitable form of multiple-quantum coherence by a preparation pulse; 2) applying phase-cycling or by using B_0 or B_1 gradient to select a particular order of multiple-quantum coherence; 3) applying another pulse train, so that the chosen multiple-quantum coherence is converted back to single-quantum coherence and becomes observable[6]. The most widely used multiple quantum filter is the double quantum filter. It is used to suppress uncoupled spin signal, especially those from the solvent. In 2-D experiments, the suppression of the diagonal peaks which arise from single quantum spins with in-phase dispersion, has two benefits: (1) eliminate the dispersion distortion to the cross peaks near the diagonal. (2) increase the dynamic range of the cross peaks[8,9].

Traditionally, multiple quantum filters are implemented by phase cycling. Phase cycling utilizes the characteristic behavior of p-quantum coherence evolution under chemical shift hamiltonian. Since a p-quantum coherence state evolves p times faster than a single quantum state, a particular quantum order will have its own evolution pathway, and can be differentiated from others. Combinations of different phase-shifted preparation pulses, mixing pulses, and detector phases will select the appropriate coherence pathways and appropriate coherence orders, and eliminate all signals other than those with the coherence order equal or higher than the selected order [6].

Multiple quantum coherence also evolves under B_0 field inhomoge-

-11-

neity. Since a p-quantum coherence experiences a p-fold dependence on the static field inhomogeneity, the higher coherence order quantum transitions are significantly broadened by the magnetic field inhomogeneity. In a gradient experiment, a single gradient pulse will dephase all the spin magnetizations that are transverse to the gradient direction. The spin states will be phase encoded with a spatially dependent term, and this phase depends on the quantum number, i.e. a p-order coherence is encoded with a phase p times larger than a single quantum coherence. The desired spins can be refocused later by a second gradient pulse or pulse train, and only those pathways for which the magnetization is fully rephased by the final gradient will contribute to the observed signal[4,5]. More specifically, in a multiple quantum filter experiment, a spin with quantum number n, along with other spins with different quantum numbers are dephased by a gradient Gn, during the mixing pulse, it undergoes a coherence transformation, and its quantum number changes from n to m. A second gradient Gm is then applied, so only spins with quantum number m are rephased.

The RF gradient method takes advantage of the RF field inhomogeneity to create a spatial averaging of nutation angles in one scan, as opposed to phase cycling which requires many scans to average out the undesired coherence pathway.

B_0 or RF gradient methods have many advantages over phase cycling procedure, following is a more detailed discussion of these advantages[2,4,5]:

(1) Great reduction in experiment time: Phase cycling inherently requires many scans to average out the undesired coherence pathways, while the gradient methods incorporate space averaging instead of time averaging,

Section 1.2

so only one experiment is needed to select the desired coherence pathway[5]. This saving in data acquistion time becomes more significant in doing multi-dimensional experiments.

(2) Significant reduction of t1 noise: In 2-D experiment, due to instrumental instabilities, the experimental conditions might vary from experiment to experiment, and there is irregular fluctuations of the signal as a function of t1[6]. The signal in $\omega 1$ dimension is modulated by t1, and t1 noise often correlates with different resonances in the $\omega 2$ domain. It is very difficult to reduce t1 noise for large signals, such as the solvent signal. Since unwanted signals are dephased from the beginning of the gradient experiments, only small signals remain. For small signals, t1 noise is approximately the same magnitude as thermal noise.

(3) Increased dynamic range: In the phase cycling procedure, to select the desired coherence pathway, the detector phase is often changed with respect to the pulse phase. In this procedure, the undesired spin states, among them the most significant is the single quantum solvent peak, followed all the way through the entire data acquisition period. The single quantum signal is suppressed only through linear combination of the FIDs from different pulse and detector phases. Due to this following through, the strong solvent peak will occupy a large part of the ADC's dynamic range. In gradient experiments, the undesired spin states are averaged out in space in a single scan instead of through linear combination of FIDs, i.e. all the undesired spin states have already been dephased by the gradient. So only the desired coherence pathway follows through the data acquisition period and it occupies the whole dynamic range.

Section 1.2

(4) Independent of field homogeneity in coherence pathway selection: We know that multiple quantum coherence evolves under B_0 field inhomogeneity Hamiltonian, which is field-dependent and also individual spectrometer-dependent. And p-quantum coherence experiences a p-fold dependence on the static field inhomogeneity $\Delta B_0(r)$.

$$\sigma p \xrightarrow{\quad -\gamma \Delta B_0 \tau I_z \quad} \sigma p \ \exp(ip\gamma\Delta B_0 \tau)$$

So the higher coherence order transitions are significantly broadened by the magnetic field inhomogeneity.

For a spin having a coherence number p, its phase is p times larger than a single quantum coherence, so the rate of evolution for this spin will be p times faster. The effects of the gradient field can be represented by the following transformation:

$$I^+ \xrightarrow{\quad \gamma I G_n \quad} I^+ \exp(-i\gamma \ G_n) = I^+ \exp(E_n)$$

$$I^- \xrightarrow{\quad \gamma I G_n \quad} I^- \exp(i\gamma \ G_n) = I^- \exp(E_n)$$

where G=gradient strength,

   τ=gradient duration.

Only those pathways for which the magnetization is fully rephased by the final gradient will contribute to the observed signal.   This can be

expressed by the general gradient equation:

$$\sum_{n} E_n = 0$$

This general gradient equation can be fulfilled for different nuclei, characterized by its gyromagnetic ratio γ, and different gradient strengths. A general n gradient homonuclar (where γ is the same) or heteronuclar experiment (where γ varies for different nuclei) can be designed to select the desired coherence pathway.

The following equation represents the transformation occurred under an RF gradient multiple quantum filter,

$$\sigma_p \xrightarrow{G_n} \sigma_p \exp(pG_n) \xrightarrow{p\rightarrow q} \sigma_q \exp(pG_n) \xrightarrow{G_m} \sigma_q \exp(pG_n) \exp t(qG_m)$$

As mentioned before, gradient methods use either a B_0 field gradient or an RF gradient. There are certain advantages of using an RF gradient instead of a B_0 field gradient. For example, a B_0 gradient is a relative restrictive method. Once the B_0 gradient is turned on, both A and B nuclei are influenced by the static gradient. By comparison, an RF gradient will dephase only A or B resonances, and the gradient experiment is relatively simple[10].

One of the most fundamental differences between a B_0 gradient and an RF gradient is that an RF gradient is non-secular[10]. Since the B_0 gradient Hamiltonian commutes with the internal Hamiltonians, the phase evolution due to internal Hamiltonians continue and extra steps must be included in the pulse sequences to refocus any additional phase shift. However, the RF gradient field is orthogonal to the internal Hamiltonians, and if the gradient is

Section 1.2

sufficiently strong, all the internal Hamiltonians will be averaged to zero. So there is no additional phase evolution during an RF gradient pulse. These characteristics make it easier and simpler to design an RF gradient experiment than a B_0 gradient experiment[4,5,10].

Chapter II

Simulations

2.1 Introduction to Coherence Transfer

To understand a 2-D COSY experiment in NMR, a key concept is coherence transfer (a transfer of specific phase relationships between spins), which is how spin-coupled nuclei interchange information under the influence of RF pulses. The following pulse sequence (Figure 2.1) is used to describe the concept of coherence transfer between two nuclei A and B that are J-coupled with a coupling constant J_{AB}[9].
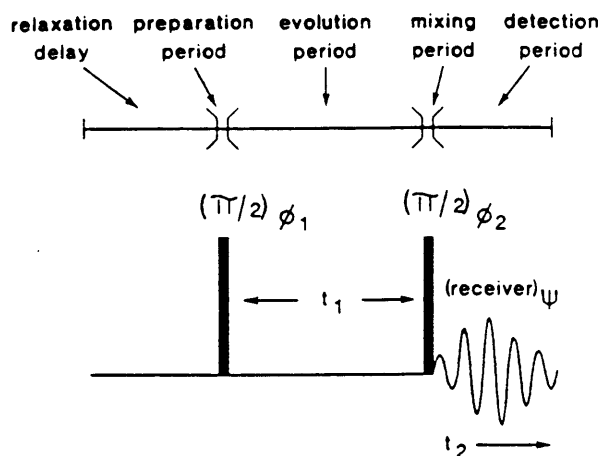

Fig. 2.1 Pulse sequence for 2D COSY. Reproduce from reference [9].

Before any pulse, A only has longitudinal magnetization. The first $\pi/2$ pulse (preparation) converts the longitudinal magnetization of A to in-phase

transverse magnetization. During the evolution period t1, the in-phase A transverse magnetization evolves into antiphase magnetization under the influence of the coupling to spin B and at a rate which depends on J_{AB}. Under the influence of the second $\pi/2$ pulse (mixing), the antiphase A transverse magnetization is converted into antiphase B transverse magnetization. Antiphase magnetization (antiphase coherence) must exist for a coherence transfer to occur, because in-phase coherence is nutated by a pulse in the same way as any other magnetization, with no coherence transfer. Since the chemical shift of nucleus A also evolves during t1, in 1-D spectroscopic experiments, it is common to insert a 180 degree pulse between the two $\pi/2$ pulses to refocus the chemical shift dephasing. After the mixing pulse, the antiphase B transverse magnetization evolves during t2 into observable in-phase B transverse magnetization, and is detected. The whole procedure can be visualized via the following vector representation (Fig. 2.2)
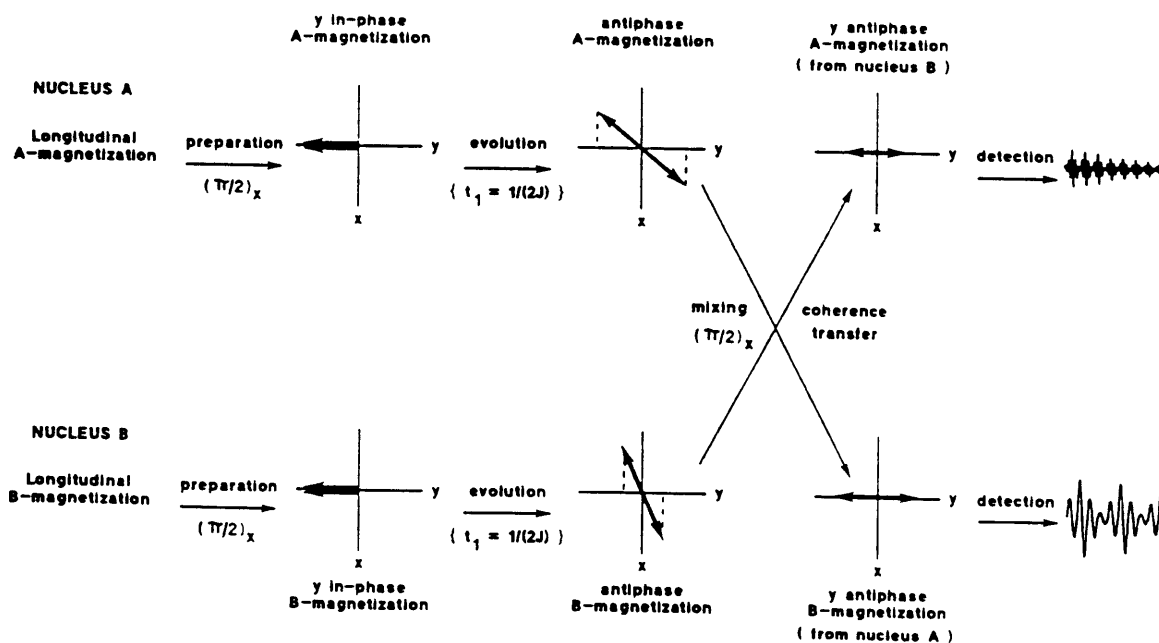

Fig. 2.2 Schematic Vector Representation of the Coherence Transfer process. Reproduce from reference [9].   Section 2.1

2.1.1 Review of Product Operator Formalism

There are three approaches for the design and analysis of new NMR techniques. They are 1) semiclassical vector models, 2) density operator theory, and 3) product operator formalism. The semiclassical vector method has inherent limitations for describing sophisticated techniques, such as multiple quantum coherence, since each spin's magnetization is followed individually and there are no formal ways of depicting higher order states. The density operator theory, can provide a full analysis for large spin system with complex pulse sequences, but usually provides little physical intuition or insights. Therefore, we use the product operator formalism for our design and analysis of the multiple quantum filters [12].

The product operator formalism is based on the density operator theory and is used to describe weakly coupled spin systems. Since it uses products of single spin angular momentum operators (I_{kz}, I_{kx}, and I_{ky}) as the basis set, this method retains the intuitive concepts of the vector models.

The following are the key concepts and basic nomenclature used in product operator formalism. The key concepts are coherence and antiphase. To describe the coherence concept, the matrix representation of the density operator has to be reviewed. In the matrix representation, a diagonal element $|r\rangle\langle r|$ is equal to the probability that the spin system is in the eigenstate $|r\rangle$. A off-diagonal element $|r\rangle\langle s|$ represents a 'coherent superposition' of eigenstates of the time-dependent Schrodinger equation,

$$\frac{d}{dt}|\Psi(t)\rangle = -iH(t)|\Psi(t)\rangle \qquad \text{section 2.1.1}$$

This superposition, also called coherence, simply means that the time dependence and the phase of the various members of the spin ensemble are correlated with respect to any pair of eigenstates, i.e. $|r\rangle$ and $|s\rangle$ [6]. The difference in magnetic quantum numbers $\Delta M = P_{rs}$, is referred to as the order of coherence, and is defined by the following equation,

$$\left[F_z, |r\rangle\langle s|\right] = p^{(rs)}|r\rangle\langle s|$$

where F_z is the total angular momentum [5]. The order of coherence P_{rs}, can take the values $-N(2I+1), \ldots, +N(2I+1)$ values in a system with N coupled spins each with spin quantum numbers I. For $P_{rs} = 0$, it is the zero-quantum coherence, with $P_{rs} = +/- 1$, it is called single-quantum coherence, etc.. Antiphase magnetization means that multiplets have individual components that have opposite phases. For example, $4I_{kx}I_{lx}I_{mz}$ has zero quantum and double quantum coherences between spin k and spin l, but with multiplet components that have opposite phases with respect to the polarization of spin m.

For one-spin product operators, they are associated with the entire spin multiples, the nomenclatures are:

I_{kz}: longitudinal magnetization of spin k,

I_{kx}: in-phase x-magnetization of spin k,

I_{ky}: in-phase y-magnetization of spin k.

For two-spin product operators:

$2I_{kx}I_{lz}$: x-magnetization of spin k antiphase with respect to spin l,

$2I_{ky}I_{lz}$: y-magnetization of spin k antiphase with respect to spin l,

$2I_{kz}I_{lz}$: longitudinal two-spin order of spins k and l (longitudinal spin order

describes the spin-correlated population of eneregy levels but without

any net polarization and observable magnetization)

$2I_{kx}I_{lx}$, $2I_{ky}I_{ly}$, and $I_{ky}I_{lx}$: two-spin coherence for spins k and l.

Figure 2.3 is a pictorial representation of product operators in a two-spin system, where $I_{kz}I_{lz}$ shows the x-magnetization of spin k antiphase with respect to spin l.
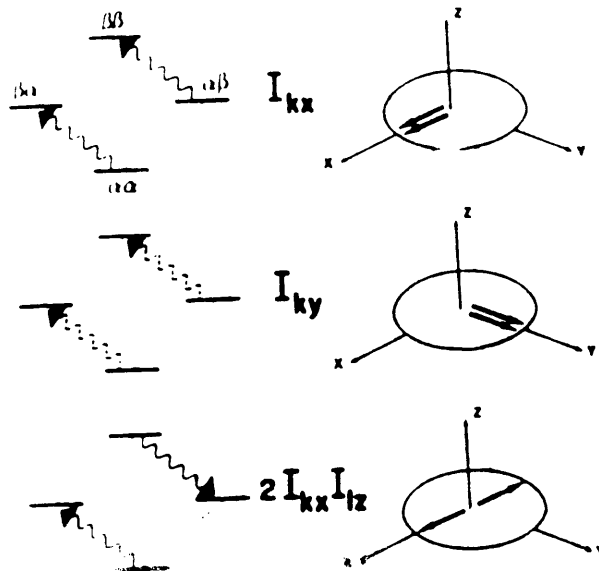

Fig. 2.3 Graphical representations of product operastors in a system of two coupled nuclei with I=1/2. Reproduce from reference [11].

For three-spin product operators with I=1/2:

$4I_{kx}I_{lz}I_{mz}$: x-magnetization of spin k in antiphase with respect to the spins l

and m,

$4I_{kx}I_{lx}I_{mz}$: two-spin coherence of spins k and l, in antiphase with respect to

spin m,

Section 2.1.1

$4I_{kx}I_{lx}I_{mx}$: three-spin coherence,

$4I_{kz}I_{lz}I_{mz}$: longitudinal three-spin order.

Now we have the nomenclature used in product operator formalsim, we can discuss the time evolution of product operators under the influence of the chemcial shift interaction, J-coupling and RF pulses.

The evolution Hamiltonian is:

$$H = \sum_{k} \Omega_k I_{kz} + \sum_{k<1} \sum 2\pi J_{kl} I_{kz} I_{lz}$$

The evoluation under chemical shift influence is:

$$I_{kx} \xrightarrow{\quad \Omega_k \tau I_{kz} \quad} I_{kx} \cos \Omega_k \tau + I_{ky} \sin \Omega_k \tau$$

$$I_{ky} \xrightarrow{\quad \Omega_k \tau I_{kz} \quad} I_{ky} \cos \Omega_k \tau - I_{kx} \sin \Omega_k \tau$$

The evolution due to spin-spin coupling is of the following:

$$I_{kx} \xrightarrow{\quad \pi J_{kl} \tau 2 I_{kz} I_{lz} \quad} I_{kx} \cos(\pi J_{kl} \tau) + 2 I_{ky} I_{lz} \sin(\pi J_{kl} \tau)$$

$$I_{ky} \xrightarrow{\quad \pi J_{kl} \tau 2 I_{kz} I_{lz} \quad} I_{ky} \cos(\pi J_{kl} \tau) - 2 I_{kx} I_{lz} \sin(\pi J_{kl} \tau)$$

The above two equations describe the conversion of in-phase magnetization into orthogonal antiphase magnetization. The following shows the opposite, from antiphase to in-phase:

$$2 I_{kx} I_{lz} \xrightarrow{\quad \pi J_{kl} \tau 2 I_{kz} I_{lz} \quad} 2 I_{kx} I_{lz} \cos(\pi J_{kl} \tau) + I_{ky} \sin(\pi J_{kl} \tau)$$

$$2 I_{ky} I_{lz} \xrightarrow{\quad \pi J_{kl} \tau 2 I_{kz} I_{lz} \quad} 2 I_{ky} I_{lz} \cos(\pi J_{kl} \tau) - I_{kx} \sin(\pi J_{kl} \tau)$$

The evolution due to radio-frequency pulses with flip angle β with rotation about the x-axis is:

$$I_{kz} \xrightarrow{\beta I_{kx}} I_{kz} \cos\beta - I_{ky} \sin\beta$$

$$I_{ky} \xrightarrow{\beta I_{kx}} I_{ky} \cos\beta + I_{kz} \sin\beta$$

Figure 2.4 shows the effect of chemical shifts, scalar couplings on product operators.

Shift or z-Pulse   x-Pulse   y-Pulse
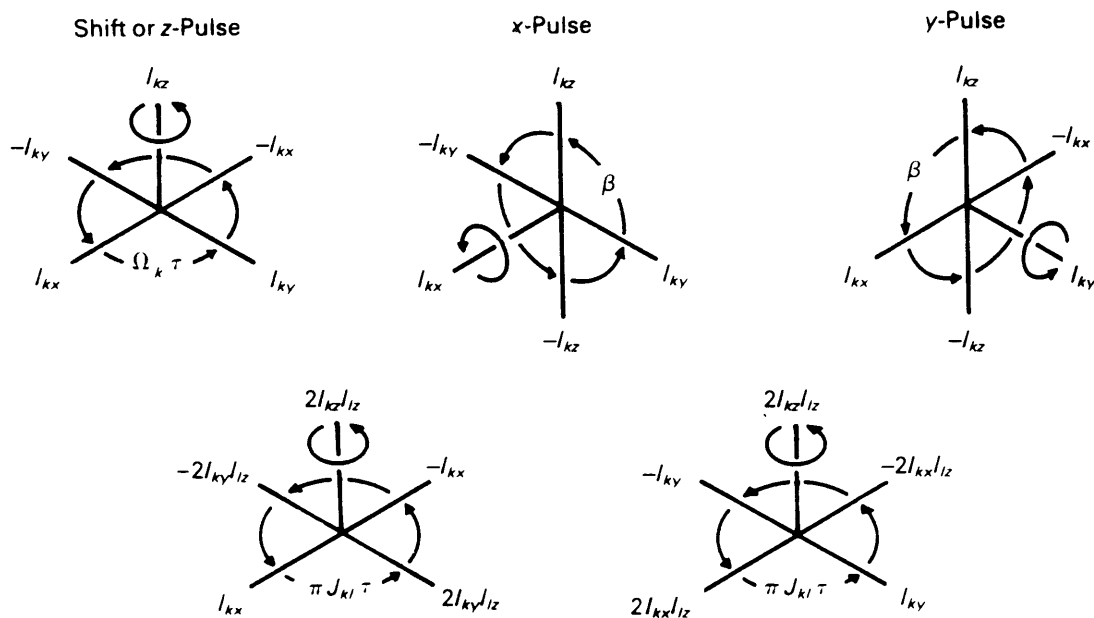
Fig. 2.4 Product Operator evolution under chemical shift (rotation about I_{kz}), R.F. pulses (rotations about I_{kx} and I_{ky}), and weak scalar coupling (rotations about $2I_{kz}I_{lz}$). Reproduce from reference [6].

Sometimes it is more convenient to consider individual coherence components I^{+} and I^{-} associated with two specific energy levels. This can be accomplished by writing I_{kx} and I_{ky} into the following:

section 2.1.1

$$I_{kx}=\frac{1}{2}(I_k^+ + I_k^-)$$

$$I_{ky}=\frac{1}{2}(I_k^+ - I_k^-)$$

The two-spin product operators can be written as:

$$2I_{kx}I_{lx}=\frac{1}{2}(I_k^+ I_l^+ + I_k^+ I_l^- + I_k^- I_l^+ + I_k^- I_l^-)$$

$$2I_{ky}I_{ly}=-\frac{1}{2}(I_k^+ I_l^+ - I_k^+ I_l^- - I_k^- I_l^+ + I_k^- I_l^-)$$

$$2I_{kx}I_{ly}=\frac{1}{2\iota}(I_k^+ I_l^+ - I_k^+ I_l^- + I_k^- I_l^+ - I_k^- I_l^-)$$

$$2I_{ky}I_{lx}=\frac{1}{2\iota}(I_k^+ I_l^+ + I_k^+ I_l^- + I_k^- I_l^+ - I_k^- I_l^-)$$

For product operators having $I_k^+ I_l^+$ or $I_k^- I_l^-$, since p=2, it is double quantum coherence. For product operators with only $I_k^+ I_l^-$ or $I_k^- I_l^+$, it is pure zero quantum coherence. Similarily, triple quantum coherence is achieved when p=3.

2.2   Simulations using POMA

Simulations are conducted on a Macintosh using POMA, a Mathematica implementation of Product Operator Formalism developed by Güntert et al. [7]. First, the phase cycling version of each of the multiple quantum filters (the double, the triple and the quadruple) are simulated. These simulations are conducted to serve as the basis for the control experiments later to be implemented on the spectrometer. Then different designs of the multiple

Section 2.2

quantum filters are simulated. The results are analyzed and the desired coherence pathways are selected. 1-D multiple quantum filters are implemented to elucidate the effectiveness of the RF gradient method and 2-D COSY experiments are then implemented to show the coherence transfer pathway and spin connectivities

2.2.1 Double Quantum Filter Simulations

A. Phase Cycling Version

1. Pulse Sequence
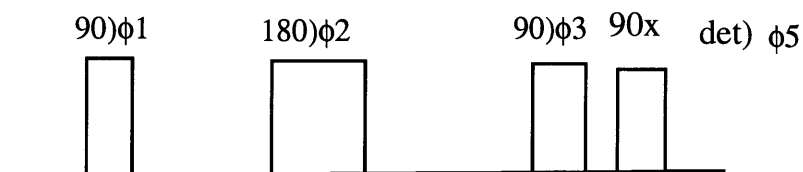
$\phi 1 = 0,180,90,270$ $\phi 3 = 0,180,90,270$

$\phi 2 = 0,180,90,270$ $det = 0,0,180,180$

2 'POMA' calculation

Source Code:

```
<< poma`
spin[1,z]//
pulse[90,{0,180,90,270}]//
delay[0.25/j[1,2],{{1,2}}]//
pulse[180,{0,180,90,270}]//
```

Section 2.2.1

delay[0.25/j[1,2],{{1,2}}]//

pulse[90,{0,180,90,270}]//

pulse[90,{0,0,0,0}]//

receiver[{0,0,180,180}]//

observable//Simplify//sort

Simulation Result:

$(I_{1z} I_{2x} + I_{1x} I_{2z})/2$

3 Analysis

This sequence is just a modification of the sequence discussed in the previous section. The first 90 degree pulse converts I_{1z} onto the transverse plane and becomes I_{1y}. The following evolution with an 180 pulse in-between the $1/4J_{12}$ time periods serves to convert the in-phase single quantum magnetization I_{1y} into a single quantum magnetization which is antiphased with respect to an active coupled spin, $I_{1x}I_{2z}$. As mentioned in section 2.1, the 180 degree pulse is used to refocus the chemical shift and the phase dispersions due to field inhomogeneity hamiltonian. The evolution time is selected according to the coupling constant J_{12}, so that most of the in-phase single quantum term evolves into anti-phase term. This can be easily observed through product operator formalism.

$I_{1x} \longrightarrow I_{1x} \cos(\pi Jt) + 2I_{1y}I_{2z} \sin(\pi Jt)$

If t=1/2J, I_{1x} will completely evolved into $I_{1y}I_{2z}$. This synchronization of all coupled spins will enhance sensitivity. However, due to dispersion of the coupling constants, this synchronization is not complete and one can only select an emperical number for practical purposes. The second 90x pulse creates double quantum coherence. $I_{1x}I_{2z}$ is converted into $I_{1x}I_{2y}$. So the pulse train, '90-1/4J-180-1/4J-90', is called a preparation pulse train, and serves to create double quantum coherence, $I_{1x}I_{2y}$, to be used for further operations. The last 90 pulse converts the double quantum $I_{1x}I_{2y}$ into antiphased single quantum $I_{1z}I_{2x}$, which evolves into observable magnetization during the detection period. The last 90 pulse is called the mixing pulse, because the single quantum magnetization of spin 1 antiphased with respect to spin 2, $I_{1x}I_{2z}$, is converted into a single quantum magnetization of spin 2 antiphased to spin 1, $I_{1z}I_{2x}$. All the pulses and the detector are phase cycled to eliminate the uncoupled single quantum spin while preserving the coupled spin magnetization.

B. Planar RF Gradient Version

1. Pulse Sequence
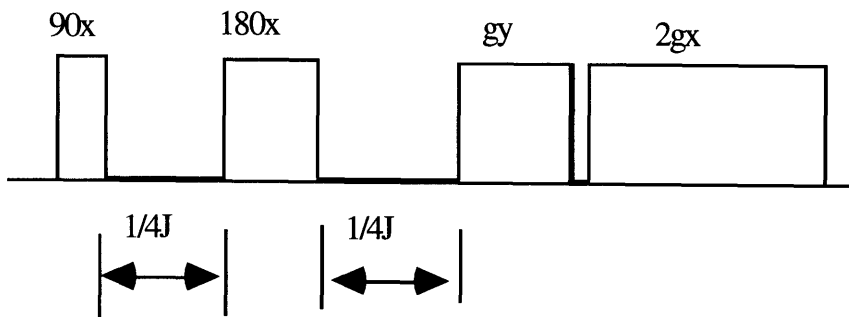
2. 'POMA' calculation

Source code:

```
<<poma`
(0.5/Pi) * Integrate[
spin[1,z]//
pulse[90,x]//
delay[0.25/j[1,2],{{1,2}}]//
pulse[180,x]//
delay[0.25/j[1,2],{{1,2}}]//
pulse[g,y]//
pulse[2g,x],{g,0,2*Pi}]//
observable//Simplify//sort
```

Result:

$-(I_{1x}I_{2z} + I_{1z} I_{2x})/4$

3 Analysis

The preparation pulse train, 90x-1/4J-180x-1/4J, is very similiar to that of the phase cycling version pulse sequence. The only difference is that the 90 pulse is omitted. The reason is the following: the antiphased term $I_{1x}I_{2z}$ is a single quantum in the ordinary definition. But in this case, both spin of $I_{1x}I_{2z}$ are transverse to the gradient direction(in this case: y), and $I_{1x}I_{2z}$ will evolve twice as fast as a single quantum term I_{1x}. The essence of the definition of p-quantum coherence is that it will evolve p times as fast as single quantum. So

Section 2.2.1

$I_{1x}I_{2z}$ is a double quantum term with respect to the Gy gradient. Therefore, the 90 pulse is no longer needed.

The double quantum term $-I_{1x}I_{2z}$ then evolves into $-I_{1x}I_{2z} \, Cos^2(\theta) + I_{1z}I_{2x} \, Sin^2(\theta)$ under the hamiltonian of Gy. Under the second gradient pulse, Gx, they evolve into $-I_{1x}I_{2z} \, Cos^2(\theta) \, Cos(2\theta) + I_{1z}I_{2x} \, Sin^2(\theta) \, Cos(2\theta)$. The spatial averaging of the nutation angle gives the following result:

$$\frac{1}{2\pi}\int_0^{2\pi} \cos^2\theta \, \cos(2\theta) d\theta = 1/4$$

$$\frac{-1}{2\pi}\int_0^{2\pi} \sin^2\theta \, \cos(2\theta) d\theta = 1/4$$

So the final result is $-(I_{1x}I_{2z} + I_{1z}I_{2x})/4$ at the end of the the pulse sequence. In the following data acquisition period, the antiphase magnetization evolved into observable magnetization.

The in-phase single quantums are eliminated by the two gradient pulses. I_x is dephased by the first gradient Gy, and I_y is spin locked by the Gy and dephased by the second gradient pulse Gx. Therefore, we don't have to worry about them.

The evolution pathway for this pulse sequence is as follows:

$$\text{Gy, 2Gx}$$
(1) I_{1z} --> (2) $-I_{1y}$ --> (3) $\{I_{1x}I_{2z}\}$ -------->(4) $-(I_{1x}I_{2z}+I_{1z}I_{2x})/4$ (evolve into observable magnetization)

$\{-I_{1y}\}$ --------> 0 (eliminated)

Section 2.2.1
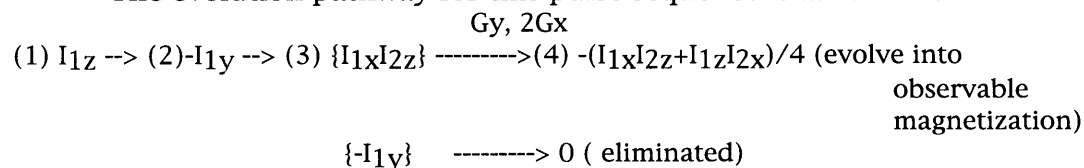
C. B$_0$ Gradient Double Quantum Filter

This sequence is for 2-D experiments. In 1-D sequence, a 180 degree pulse is used in between the 2 90x pulses to refocus chemical shift effects. Since we want to utilize the chemical shift effect in 2-D experiments, the 180 degree pulse is eliminated.

1 Pulse Sequence:
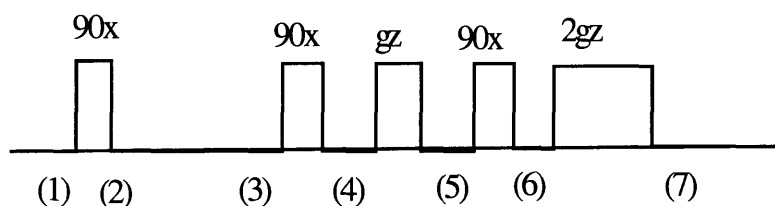
2. 'POMA' calculation

Source code:

```
(0.5/Pi) * Integrate[spin[1,z]//
pulse[90,x]//
delay[t1,{{1,2}}]//
pulse[90,x]//
pulse[g,z]//
pulse[90,x]//
pulse[2g,z],{g,0,2*Pi}]//
observable//Simplify//sort
```

Result:

$-(I_{1x}I_{2z}+I_{1z}I_{2x})/4$ Section 2.2.1

3 Analysis

The first 90 pulse excites the spin system. and create four states, I_{1x}, I_{1y}, $I_{1x}I_{2z}$, $I_{1y}I_{2z}$. I_{1x}, I_{1y}, $I_{1y}I_{2z}$ are all dephased by the following pulses and B0 gradients, while $I_{1x}I_{2z}$ is dephased and then refocused, therefore it is preserved. The coherence pathway is as the following:

(3) I_{1x}--->(4) I_{1x}--->(5)$I_{1x}Cos(\theta)+I_{1y}Sin(\theta)$--->(6)$I_{1x} Cos(\theta)+I_{1y} Sin(\theta)$

--->(7)$-I_{1y} Cos(2\theta)+I_{1x} Sin(2\theta)$ ---> $\int_0^{2\pi} d\theta = 0$

(3) I_{1y}---> (4) I_{1z}--->(5) I_{1z}--->(6) $-I_{1y}$--->(7) $-I_{1y} Cos(2\theta)+I_{1x} Sin(2\theta)$

---> $\int_0^{2\pi} d\theta = 0$

(3) $I_{1x}I_{2z}$--->(4)$I_{1x}I_{2y}$--->(5) $-I_{1x}I_{2y}Cos^2(\theta)+I_{1y}I_{2x}Sin^2(\theta)$

--->(6) $-I_{1x}I_{2z}Cos^2(\theta)+I_{1z}I_{2x}Sin^2(\theta)$

--->(7) $I_{1z}I_{2x}Cos(2\theta)Sin^2(\theta) +I_{1z}I_{2y}Sin(2\theta)Sin^2(\theta) -I_{1x}I_{2z}Cos(2\theta)Cos^2(\theta)$

$-I_{1y}I_{2z}Sin(2\theta)Cos^2(\theta)$ ---> $\int_0^{2\pi} d\theta = -(I_{1x}I_{2z}+I_{1z}I_{2x})/4$

(3) $I_{1y}I_{2z}$--->(4) $-I_{1z}I_{2y}$--->(5)$-I_{1z}I_{2y}Cos(\theta)+I_{1z}I_{2x}Sin(\theta)$

--->(6)$I_{1y}I_{2z}Cos(\theta)$--->(7)$I_{1y}I_{2z}Cos(2\theta)Cos(\theta)-I_{1x}I_{2z}Sin(2\theta)Cos(\theta)$

---> $\int_0^{2\pi} d\theta = 0$

Section 2.2.1

D. Planar RF gradient Double Quantum Filter

Again, this is a 2-D sequence, so the 180 degree refocusing pulse for chemical shift is eliminated.

1 Pulse Sequence:
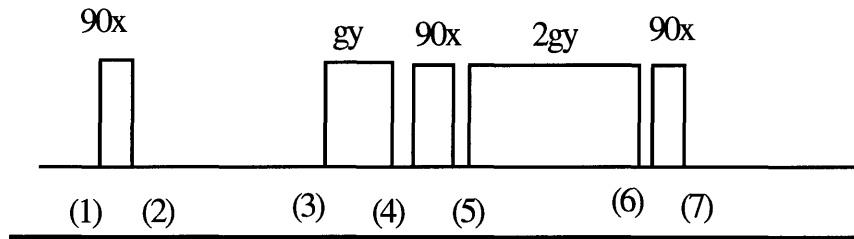
2. 'POMA' calculation

Source code:

```
(0.5/Pi) * Integrate[spin[1,z]//

pulse[90,x]//

delay[t1,{{1,2}}]//

pulse[g,y]//

pulse[90,x]//

pulse[2g,y]//

pulse[90,x],{g,0,2*Pi}]//

observable//Simplify//sort
```

Result:

$-(I_{1z} I_{2x} + I_{1x} I_{2z})/4$

Section 2.2.1

-32-

3 Analysis

The first 90 pulse excites the spin system. And antiphased terms, $I_{1x}I_{2z}$ and $I_{1y}I_{2z}$, as well as in-phased I_{1x} and I_{1y} occur during the evolution. $I_{1x}I_{2z}$ is the double quantum term for the first Gy gradient. It evolves through the following pulse and gradient sequences and is preserved. All the other three terms are dephased by the following pulse and gradient train. The detailed evolution pathway is as the following:

(3) $I_{1x}I_{2z}$---> (4) $I_{1x}I_{2z}\,Cos^2(\theta)-I_{1z}I_{2x}Sin^2(\theta)$

--->(5)$-I_{1x}I_{2y}Cos^2(\theta)+I_{1y}I_{2x}Sin^2(\theta)$

--->(6) $-I_{1x}I_{2y}Cos(2\theta)Cos^2(\theta) +I_{1z}I_{2y}Sin(2\theta)Cos^2(\theta)-I_{1y}I_{2z}Sin(2\theta)Sin^2(\theta)$

$+I_{1y}I_{2x}Cos(2\theta)Sin^2(\theta)$

--->(7) $-I_{1x}I_{2z}Cos(2\theta)Cos^2(\theta) -I_{1y}I_{2z}Sin(2\theta)Cos^2(\theta) +I_{1z}I_{2y}Sin(2\theta)Sin^2(\theta)$

$+I_{1z}I_{2x}Cos(2\theta)Sin^2(\theta)$

$---> \int_0^{2\pi} d\theta = -(I_{1x}I_{2z}+ I_{1z}I_{2x})/4$

(3) I_{1x}--->(4) $I_{1x}Cos(\theta)-I_{1z}Sin(\theta)$--->(5) $I_{1x}Cos(\theta) +I_{1y}Sin(\theta)$

---> (6) $I_{1x}Cos(2\theta)Cos(\theta) -I_{1z}Sin(2\theta)Cos(\theta) +I_{1y}Sin(\theta)$

--->(7) $I_{1x}Cos(2\theta)Cos(\theta) +I_{1y}Sin(2\theta)Cos(\theta) +I_{1z}Sin(\theta)$---> $\int_0^{2\pi} d\theta=0$

(3) I_{1y}--->(4) I_{1y}--->(5) I_{1z}--->(6) $I_{1z}Cos(2\theta)+I_{1x}Sin(2\theta)$

--->(7) $-I_{1y}Cos(2\theta) +I_{1x}Sin(2\theta)$---> $\int_0^{2\pi} d\theta=0$

(3) $I_{1y}I_{2z}$--->(7) $I_{1x}I_{2z}Sin(2\theta)Cos(\theta) +I_{1y}I_{2z}Cos(2\theta)Cos(\theta)$---> $\int_0^{2\pi} d\theta=0$

Section 2.2.1

E.Planar Gradient Double Quantum Filter

Again, the 180 degree pulse is left out of the 2-D pulse sequence.
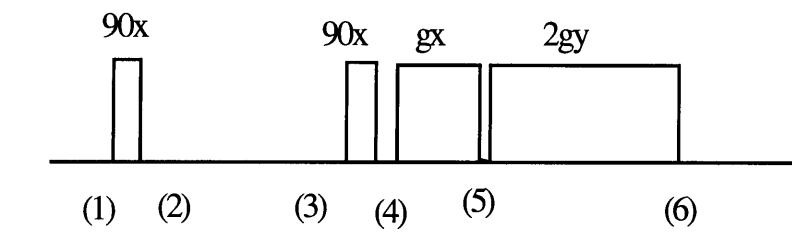
1. Pulse Sequence:

2. 'POMA' calculation

Source code:

```
(0.5/Pi) * Integrate[spin[1,z]//

pulse[90,x]//

delay[t1,{{1,2}}]//

pulse[90,x]//

pulse[g,x]//

pulse[2g,y],{g,0,2*Pi}]//

observable//Simplify//sort
```

Result:

$-(I_{1z} I_{2y} + I_{1y} I_{2z})/4$

3 Analysis:

As before, the first 90 pulse excites the spin system. The magnetization evolves under the chemical shift and J -coupling Hamiltonians. So there are

four terms developed during this period: I_{1x}, I_{1y}, $I_{1x}I_{2z}$, $I_{1y}I_{2z}$. The following pulse and gradient train will destroy I_{1x}, I_{1y}, $I_{1x}I_{2z}$ and preserve only $I_{1y}I_{2z}$. The detailed evolution pathways are the following:

(3) I_{1x}--->(4) I_{1x}--->(5) I_{1x}--->(6) $I_{1x}Cos(2\theta)-I_{1z}Sin(2\theta)$---> $\int_0^{2\pi} d\theta=0$

(3) I_{1y}--->(4) I_{1z}--->(5) $I_{1z}Cos(\theta)-I_{1y}Sin(\theta)$--->(6) $I_{1x}Sin(2\theta)Cos(\theta)$ $-I_{1y}Sin(\theta)$
---> $\int_0^{2\pi} d\theta=0$

(3)$I_{1x}I_{2z}$--->(4) $-I_{1x}I_{2y}$--->(5) $-I_{1x}I_{2y}Cos(\theta)-I_{1x}I_{2z}Sin(\theta)$
--->(6) $I_{1z}I_{2y}Sin(2\theta)Cos(\theta)-I_{1x}I_{2z}Cos^2(2\theta)Sin(2\theta)+I_{1z}I_{2x}Sin^3(2\theta)$---> $\int_0^{2\pi} d\theta=0$

(3)$I_{1y}I_{2z}$--->(4) $-I_{1z}I_{2y}$--->(5) $-I_{1z}I_{2y}Cos^2(\theta)+I_{1y}I_{2z}Sin^2(\theta)$
--->(6) $-I_{1z}I_{2y}Cos(2\theta)Cos^2(\theta)$ $+I_{1y}I_{2z}Cos(2\theta)Sin^2(\theta)$
---> $\int_0^{2\pi} d\theta=-(I_{1z}I_{2y}+I_{1y}I_{2z})/4$

As mentioned before, only $I_{1y}I_{2z}$ will evolve into observable magnetization.

2.2.2 Triple Quantum Filter Simulations

A. Phase Cycling Version

As before, the 180 degree pulse is eliminated in the 2-D pulse sequence.

1. Pulse Sequence:
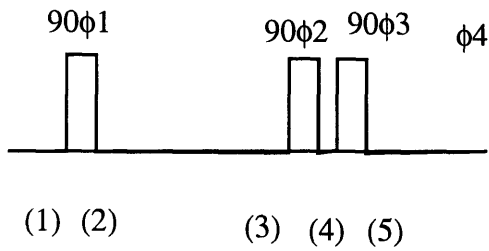
Phase Cycle:

$\phi1$= 0, 60, 120, 180, 240, 300

$\phi2$= 0, 60, 120, 180, 240, 300

$\phi3$= 0, 0, 0, 0, 0, 0

$\phi4$= 0, 180, 0, 180, 0, 180

2. 'POMA' calculation.

Source Code:

```
spin[1,z]//

pulse[90,{0,60,120,180,240,300}]//

delay[t1,{{1,2},{1,3}}]//

pulse[90,{0,60,120,180,240,300}]//

pulse[90,{0,0,0,0,0,0}]//

receiver[{0,180,0,180,0,180}]//

observable//Simplify//sort
```

Result:

$-(I_{1x}I_{2z}I_{3z} + I_{1z}I_{2z}I_{3x} + I_{1z}I_{2x}I_{3z})/4$

Section 2.2.2

B. 1-D Planar RF Gradient Version 1

(2-D sequence, without 180 degree pulse)

1. Pulse Sequence
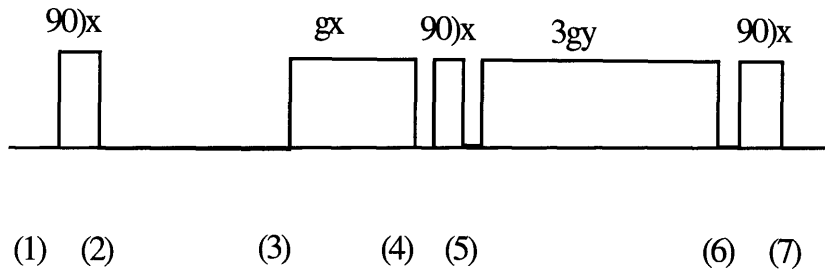
2. 'POMA' calculation

Source Code:

```
<<poma`

Integrate[spin[1,z]//

pulse[90,x]//

delay[t1,{{1,2},{1,3}}]//

pulse[g,x]//

pulse[90,x]//

pulse[3g,y]//

pulse[90,x],{g,0,2*Pi}]//

observable//Simplify//sort
```

Result:

$-(I_{1y} I_{2z} I_{3z} + I_{1z} I_{2z} I_{3y} + I_{1z} I_{2y} I_{3z})/8$

Section 2.2.2

3. Analysis

The first 90 pulse excites all the spins into the transverse plane. The following time delay prepares the system into several spin states: I_{1x}, I_{1y}, $I_{1x}I_{2z}$, $I_{1y}I_{2z}$, $I_{1x}I_{2z}I_{3z}$, $I_{1y}I_{2z}I_{3z}$. Since $I_{1y}I_{2z}I_{3z}$ will evolve three times as fast as a single quantum under the gradient hamiltonian, it is a triple quantum term for gradient pulse gx. This triple quantum term is preserved through the following pulse sequence and evolves into observable magnetization, while the single quantum coherences and double quantum coherences are destroyed by the gradient pulses. The detailed pathway for $I_{1y}I_{2z}I_{3z}$ is as follows:

(1) I_{1z}--->(2)-I_{1y}--->(3) $I_{1y}I_{2z}I_{3z}$

--->(4) $I_{1y}I_{2z}I_{3z}Cos^3(\theta)$ -$I_{1z}I_{2y}I_{3z}Cos(\theta) Sin^2(\theta)$ - $I_{1z}I_{2z}I_{3y}Cos(\theta) Sin^2(\theta)$

--->(5) $I_{1z}I_{2y}I_{3y}Cos^3(\theta)$ - $I_{1y}I_{2z}I_{3y}Cos(\theta) Sin^2(\theta)$ - $I_{1y}I_{2y}I_{3z}Cos(\theta) Sin^2(\theta)$

--->(6) $I_{1z}I_{2y}I_{3y}Cos^3(\theta) Cos(3\theta)$ - $I_{1y}I_{2z}I_{3y}Cos(\theta) Sin^2(\theta) Cos(3\theta)$ - $I_{1y}I_{2y}I_{3z}Cos(\theta) Sin^2(\theta) Cos(3\theta)$

--->(7) $-I_{1y}I_{2z}I_{3z}Cos^3(\theta) Cos(3\theta)$ + $I_{1z}I_{2y}I_{3z}Cos(\theta)Sin^2(\theta) Cos(3\theta)$ + $I_{1z}I_{2z}I_{3y}Cos(\theta) Sin^2(\theta) Cos(3\theta)$

--->$\int_0^{2\pi} d\theta$=-$(I_{1y}I_{2z}I_{3z} + I_{1z}I_{2z}I_{3y} + I_{1z}I_{2y}I_{3z})/8$

C. 1-D Planar RF Gradient Version 2

1. Pulse Sequence

(1)   (2)   (3)   (4)   (5)

2. 'POMA' calculation

Source Code:

```
Integrate[

spin[1,z]//

pulse[90,x]//

delay[t1,{{1,2},{1,3}}]//

pulse[2g,x]//

pulse[3g,y],{g,0,2*Pi}]//

observable//Simplify//sort
```

Result:

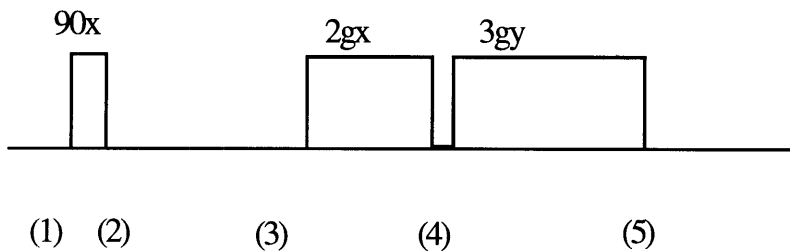$(I_{1z}I_{2z}I_{3y} + I_{1z}I_{2y}I_{3z} + I_{1y}I_{2z}I_{3z})/16$

3. Analysis:

This is a second version of triple quantum filter implemented through planar RF gradients. By using 2gx instead of 1gx, it can achieve the same coherence order selection but with using less pulses. The detailed coherence pathway is as follows:

(1) I_{1z}--->(2) $-I_{1y}$--->(3) $I_{1y}I_{2z}I_{3z}$

--->(4) $I_{1y}I_{2z}I_{3z}Cos^3(2\theta)$ $- I_{1z}I_{2y}I_{3z}Cos(2\theta) Sin^2(2\theta) - I_{1z}I_{2z}I_{3y}Cos(2\theta) Sin^2(2\theta)-$

--->(5) $I_{1y}I_{2z}I_{3z}Cos^3(2\theta) Cos^2(3\theta) - I_{1z}I_{2y}I_{3z}Cos(2\theta) Sin^2(2\theta)Cos^2(3\theta)-$

$I_{1z}I_{2z}I_{3y}Cos(2\theta) Sin^2(2\theta)Cos^2(3\theta)$

---> $\int_0^{2\pi} d\theta$ = $(I_{1z}I_{2z}I_{3y}+ I_{1z}I_{2y}I_{3z} + I_{1y}I_{2z}I_{3z})/16$

Section 2.2.2

Therefore, from the simulations, we know that there are different ways to achieve the desired quantum states.

2.2.3. Quadruple Quantum Filter Simulations

A. Phase Cycling Version

(2-D sequence, so 180 degree chemical shift refocusing pulse is elminated)

1. Pulse Sequence:
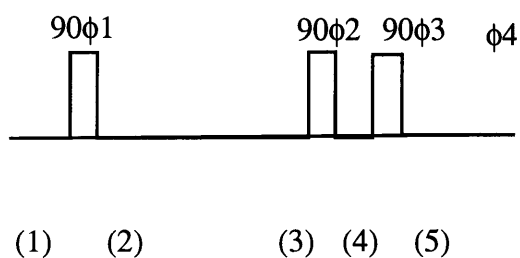
Phase Cycle:

$\phi1=0,45,90,135,180,225,270,315$

$\phi2=0,45,90,135,180,225,270,315$

$\phi3=0,0,0,0,0,0$

$\phi4=0,180,0,180,0,180$

2. 'POMA' calculation

Source Code:

```
spin[1,z]//
pulse[90,{0,45,90,135,180,225,270,315}]//
delay[t1,{{1,2},{1,3},{1,4}}]//
pulse[90,{0,45,90,135,180,225,270,315}]//
pulse[90,{0,0,0,0,0,0,0,0}]//
```

receiver[{0,180,0,180,0,180,0,180}]//

observable//Simplify//sort

Result:

$(I_{1z}I_{2z}I_{3z}I_{4x} + I_{1z}I_{2z}I_{3x}I_{4z} + I_{1z}I_{2x}I_{3z}I_{4z} + I_{1x}I_{2z}I_{3z}I_{4z})/8$

B. Planar RF Gradient Version 1

1. Pulse Sequence:
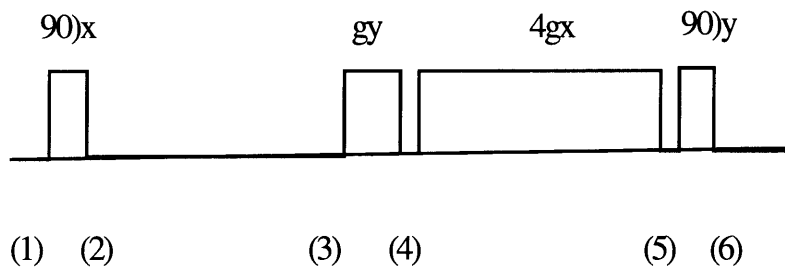
2.'POMA' calculation

Source Code:

```
Integrate[

spin[1,z]//

pulse[90,x]//

delay[t1,{{1,2},{1,3},{1,4}}]//

pulse[g,y]//

pulse[4g,x]//

pulse[90,y],{g,0,2*Pi}]//

observable//Simplify//sort
```

Section 2.2.3

Result:

$(I_{1x}I_{2z}I_{3z}I_{4z} + I_{1z}I_{2x}I_{3z}I_{4z} + I_{1z}I_{2z}I_{3x}I_{4z} + I_{1z}I_{2z}I_{3z}I_{4x})/16$

3. Analysis

The preparation pulse excites the spin system and build up four quantum spin $I_{1x}I_{2z}I_{3z}I_{4z}$, which is preserved through the gradient pulse train and later on evolves into observable magnetization. All the rest of the terms, i.e. I_{1x}, I_{1y}, $I_{1x}I_{2z}$, $I_{1y}I_{2z}$, $I_{1x}I_{2z}I_{3z}$, $I_{1y}I_{2z}I_{3z}$, $I_{1y}I_{2z}I_{3z}I_{4z}$, are dephased by the following pulses and gradients train. The detailed pathway is as follows:

$(1)\ I_{1z} \longrightarrow (2)\ -I_{1y} \longrightarrow (3) I_{1x}I_{2z}I_{3z}I_{4z}$

$\longrightarrow (4)\ -I_{1z}I_{2x}I_{3x}I_{4x}Sin^4(\theta)\ + I_{1x}I_{2z}I_{3x}I_{4x}Sin^2(\theta)\ Cos^2(\theta) +$

$I_{1x}I_{2x}I_{3z}I_{4x}Sin^2(\theta)\ Cos^2(\theta) + I_{1x}I_{2x}I_{3x}I_{4z}Sin^2(\theta)\ Cos^2(\theta)$

$\longrightarrow (5)\ -I_{1z}I_{2x}I_{3x}I_{4x}Sin^4(\theta)\ Cos(4\theta) + I_{1x}I_{2z}I_{3x}I_{4x}Sin^2(\theta)\ Cos^2(\theta)Cos(4\theta) +$

$I_{1x}I_{2x}I_{3z}I_{4x}Sin^2(\theta)\ Cos^2(\theta)Cos(4\theta) + I_{1x}I_{2x}I_{3x}I_{4z}Sin^2(\theta)\ Cos^2(\theta)Cos(4\theta)$

$\longrightarrow (6)\ I_{1z}I_{2x}I_{3x}I_{4x}Sin^4(\theta)\ Cos(4\theta) - I_{1x}I_{2z}I_{3x}I_{4x}Sin^2(\theta)\ Cos^2(\theta)Cos(4\theta) -$

$I_{1x}I_{2x}I_{3z}I_{4x}Sin^2(\theta)\ Cos^2(\theta)Cos(4\theta) - I_{1x}I_{2x}I_{3x}I_{4z}Sin^2(\theta)\ Cos^2(\theta)Cos(4\theta)$

$\longrightarrow \int_0^{2\pi} d\theta = (I_{1x}I_{2z}I_{3z}I_{4z} + I_{1z}I_{2x}I_{3z}I_{4z} + I_{1z}I_{2z}I_{3x}I_{4z} + I_{1z}I_{2z}I_{3z}I_{4x})/16$

C. Planar RF Gradient Version 2

1. Pulse Sequence:

2. 'POMA' calculation

Source Code:

```
Integrate[

spin[1,z]//

pulse[90,x]//

delay[t1,{{1,2},{1,3},{1,4}}]//

pulse[3g,y]//

pulse[4g,x],{g,0,2*Pi}]//

observable//Simplify//sort
```

Result:

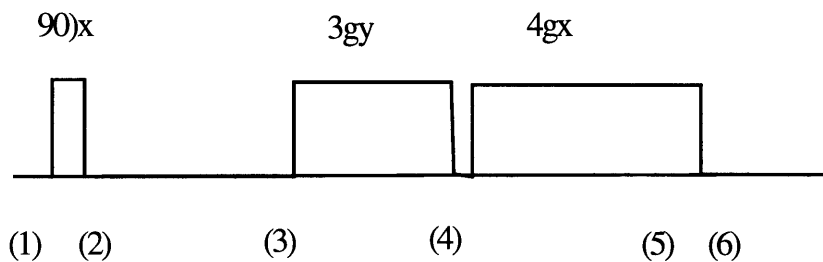$(I_{1x}I_{2z}I_{3z}I_{4z}+I_{1z}I_{2x}I_{3z}I_{4z}+I_{1z}I_{2z}I_{3x}I_{4z}+I_{1z}I_{2z}I_{3z}I_{4x})/64$

3. Analysis

The first 90 pulse build up the antiphased term $I_{1x}I_{2z}I_{3z}I_{4z}$, which is a four quantum with respect to the first gradient, Gy. This four quantum term will evolve through the next two gradients and become observable during data acquisition. All other terms that have been built up during the evolution time interval t1, i.e., I_{1x}, I_{1y}, $I_{1x}I_{2z}$, $I_{1y}I_{2z}$, $I_{1x}I_{2z}I_{3z}$, $I_{1y}I_{2z}I_{3z}$, $I_{1y}I_{2z}I_{3z}I_{4z}$ are dephased by the two succeeding RF gradient pulses. The detailed pathway of the selection is as follows:

(1) I_{1z}-->(2) $-I_{1y}$-->(3) $I_{1x}I_{2z}I_{3z}I_{4z}$--->(4) $I_{1x}I_{2z}I_{3z}I_{4z}Cos^4(3\theta)$ +

$(I_{1z}I_{2x}I_{3z}I_{4z}+I_{1z}I_{2z}I_{3x}I_{4z}+I_{1z}I_{2z}I_{3z}I_{4x})Sin^2(3\theta)$ $Cos^2(3\theta)$

---> (5)$I_{1x}I_{2z}I_{3z}I_{4z}Cos^4(3\theta)$ $Cos^3(4\theta)$+

$(I_{1z}I_{2x}I_{3z}I_{4z}+I_{1z}I_{2z}I_{3x}I_{4z}+I_{1z}I_{2z}I_{3z}I_{4x})Sin^2(3\theta)$ $Cos^2(3\theta)Cos^3(4\theta)$

---> $\int_0^{2\pi}d\theta=(I_{1x}I_{2z}I_{3z}I_{4z}+I_{1z}I_{2x}I_{3z}I_{4z}+I_{1z}I_{2z}I_{3x}I_{4z}+I_{1z}I_{2z}I_{3z}I_{4x})/64$

From the pulse sequences and simulations presented above, it can be seen that RF gradient should function well in multiple quantum filtered experiments. The use of Rf gradients eliminate the need for phase cycling and reduces the experiment to single scan acquisition.

Section 2.2.3

2.3 Summary of Coherence Transfer Pathways

Since we are using the residual inhomogeneity of the B0 field to serve as the RF gradient, only the planar RF gradient pulse sequences will be implemented on the spectrometer. Table 2.1 lists the Double Quantum Filter pathways, table 2.2 lists the two Triple Quantum Filter pathways, and table 2.3 shows the two Quadruple Quantum Filter pathways.

Table 2.1 Double Quantum Filter Pathways

A. Double Quantum Filter version 1: 90x-1/4J-180x-1/4J-Gy-2Gx

$$
\begin{array}{cccccccc}
 & & I_{1x} & & & & & 0 \\
90x & t1 & -I_{1y} & Gy & 2Gx & \int_0^{2\pi} d\theta & & 0 \\
\end{array}
$$

$$
I_{1z} \longrightarrow -I_{1y} \longrightarrow 2I_{1x}I_{2z} \longrightarrow \longrightarrow \longrightarrow -(2I_{1x}I_{2z} + 2I_{1z}I_{2x})/4
$$

$$
2I_{1y}I_{2z} \qquad\qquad 0
$$

B. Double Quantum Filter version 2: 90x-1/2J-Gy-90x-2Gy-90x

$$
\begin{array}{ccccccccc}
 & & I_{1x} & & & & & & 0 \\
90x & t1 & -I_{1y} & Gy & 90x & 2Gy & 90x & \int_0^{2\pi} d\theta & 0 \\
\end{array}
$$

$$
I_{1z} \longrightarrow -I_{1y} \longrightarrow 2I_{1x}I_{2z} \longrightarrow \longrightarrow \longrightarrow \longrightarrow -(2I_{1x}I_{2z} + 2I_{1z}I_{2x})/4
$$

$$
2I_{1y}I_{2z} \qquad\qquad 0
$$

C. Double Quantum Filter version 3: 90x-1/2J-90x-Gx-2Gy

$$
\begin{array}{ccccccccc}
 & & I_{1x} & & I_{1x} & & & & 0 \\
90x & t1 & -I_{1y} & 90x & -I_{1z} & Gx & 2Gy & \int_0^{2\pi} d\theta & 0 \\
\end{array}
$$

$$
I_{1z} \longrightarrow -I_{1y} \longrightarrow 2I_{1x}I_{2z} \longrightarrow -2I_{1x}I_{2y} \longrightarrow \longrightarrow \longrightarrow -(2I_{1z}I_{2y} + 2I_{1y}I_{2z})/4
$$

$$
2I_{1y}I_{2z} \qquad -2I_{1z}I_{2y} \qquad\qquad 0
$$

Table 2.2 Triple Quantum Filter Pathways

A. Triple Quantum Filter version 1: 90x-1/2J-Gx-90x-3Gy-90x

			I_{1x}					0
90x	t1		$-I_{1y}$	Gx	90x 3Gy 90x	$\int_0^{2\pi} d\theta$		0

$I_{1z} \longrightarrow -I_{1y} \longrightarrow 2I_{1x}I_{2z} \longrightarrow \longrightarrow \longrightarrow \longrightarrow \longrightarrow$ ... 0

$\qquad\qquad\qquad\quad 2I_{1y}I_{2z}$ ... 0

$\qquad\qquad\qquad\quad 4I_{1x}I_{2z}I_{3z}$ ... 0

$\qquad\qquad\qquad\quad 4I_{1y}I_{2z}I_{3z}$ ... $-(4I_{1y}I_{2z}I_{3z} + 4I_{1z}I_{2z}I_{3y} + 4I_{1z}I_{2y}I_{3z})/8$

B. Triple Quantum Filter version 2: 90x-1/2J-2Gx-3Gy

			I_{1x}					0
90x	t1		$-I_{1y}$	2Gx	3Gy	$\int_0^{2\pi} d\theta$		0

$I_{1z} \longrightarrow -I_{1y} \longrightarrow 2I_{1x}I_{2z} \longrightarrow \longrightarrow \longrightarrow$ ... 0

$\qquad\qquad\qquad\quad 2I_{1y}I_{2z}$ ... 0

$\qquad\qquad\qquad\quad 4I_{1x}I_{2z}I_{3z}$ ... 0

$\qquad\qquad\qquad\quad 4I_{1y}I_{2z}I_{3z}$ ... $(4I_{1y}I_{2z}I_{3z} + 4I_{1z}I_{2z}I_{3y} + 4I_{1z}I_{2y}I_{3z})/16$

Section 2.3

Table 2.3 Quadruple Quantum Filter Pathways

A. Quadruple Quantum Filter version 1: 90x-1/2J-Gy-4Gx-90y

$$I_{1x} \qquad\qquad\qquad\qquad 0$$

$$90x \quad t1 \quad -I_{1y} \quad Gy \quad 4Gx \quad 90y \int_0^{2\pi} d\theta \qquad 0$$

$I_{1z} \longrightarrow -I_{1y} \longrightarrow 2I_{1x}I_{2z} \; \dashrightarrow \; \dashrightarrow \; \dashrightarrow \; \dashrightarrow \qquad\qquad 0$

$\qquad\qquad\qquad\qquad 2I_{1y}I_{2z} \qquad\qquad\qquad\qquad\qquad 0$

$\qquad\qquad\qquad\qquad 4I_{1x}I_{2z}I_{3z} \qquad\qquad\qquad\qquad\qquad 0$

$\qquad\qquad\qquad\qquad 4I_{1y}I_{2z}I_{3z} \qquad\qquad\qquad\qquad\qquad 0$

$\qquad\qquad\qquad\qquad 8I_{1y}I_{2z}I_{3z}I_{4z} \qquad\qquad\qquad\qquad 0$

$\qquad\qquad\qquad\qquad 8I_{1x}I_{2z}I_{3}I_{4z} \qquad\qquad\qquad (8I_{1x}I_{2z}I_{3z}I_{4z}+8\,I_{1z}I_{2x}I_{3z}I_{4z}+$

$$8I_{1z}I_{2z}I_{3x}I_{4z}+ 8I_{1z}I_{2z}I_{3z}I_{4x})/16$$

B. Quadruple Quantum Filter version 2: 90x-1/2J-3Gy-4Gx

$$I_{1x} \qquad\qquad\qquad\qquad 0$$

$$90x \quad t1 \quad -I_{1y} \quad 3Gy \quad 4Gx \int_0^{2\pi} d\theta \qquad 0$$

$I_{1z} \longrightarrow -I_{1y} \longrightarrow 2I_{1x}I_{2z} \; \dashrightarrow \; \dashrightarrow \; \dashrightarrow \qquad\qquad 0$

$\qquad\qquad\qquad\qquad 2I_{1y}I_{2z} \qquad\qquad\qquad\qquad\qquad 0$

$\qquad\qquad\qquad\qquad 4I_{1x}I_{2z}I_{3z} \qquad\qquad\qquad\qquad\qquad 0$

$\qquad\qquad\qquad\qquad 4I_{1y}I_{2z}I_{3z} \qquad\qquad\qquad\qquad\qquad 0$

$\qquad\qquad\qquad\qquad 8I_{1y}I_{2z}I_{3z}I_{4z} \qquad\qquad\qquad\qquad 0$

$\qquad\qquad\qquad\qquad 8I_{1x}I_{2z}I_{3}I_{4z} \qquad\qquad\qquad (8I_{1x}I_{2z}I_{3z}I_{4z}+ 8I_{1z}I_{2x}I_{3z}I_{4z}+$
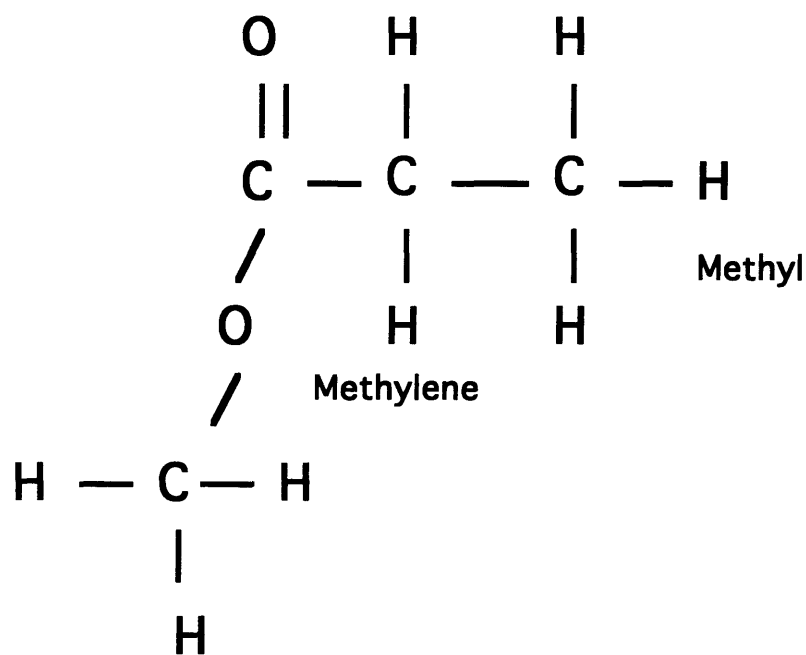
$$8I_{1z}I_{2z}I_{3x}I_{4z}+ 8I_{1z}I_{2z}I_{3z}I_{4x}/16$$

Chapter III

NMR Experiments

The experiments were conducted on a Bruker 400 MHz spectometer. The sample used was ethyl acetate in deuterated acetone. To serve as a control, the ethyl acetate spectrum were first taken with a single 90 degree excitation pulse, which is approximately 9.5 micro-seconds for the specific probe we used and the spectrometer mentioned above. The structure of ethyl acetate is as follows:

$$
\begin{array}{ccccccc}
\text{O} & & \text{H} & & \text{H} & & \\
\parallel & & | & & | & & \\
\text{C} & - & \text{C} & - & \text{C} & - & \text{H} \\
\diagup & & | & & | & & \text{Methyl} \\
\text{O} & & \text{H} & & \text{H} & & \\
\diagup & & \text{Methylene} & & & & \\
\end{array}
$$

$$
\text{H} - \text{C} - \text{H}
$$
$$
|
$$
$$
\text{H}
$$

Acetate

Figure 3.1 shows the ethyl acetate spectrum without any multiple quantum filtering. The single peak comes from the acetate, the triplet comes from the methyl group, and the quartet comes from the methylene.

ETHYL ACETATE SPECTRUM WITH NO FILTER

BRUKER

EACETATE.002

PW   9.0

acetate

methyl

methylene

| 6200 | 6000 | 5800 | 5600 | 5400 | 5200 | 5000 | 4800 | 4600 |

HERTZ
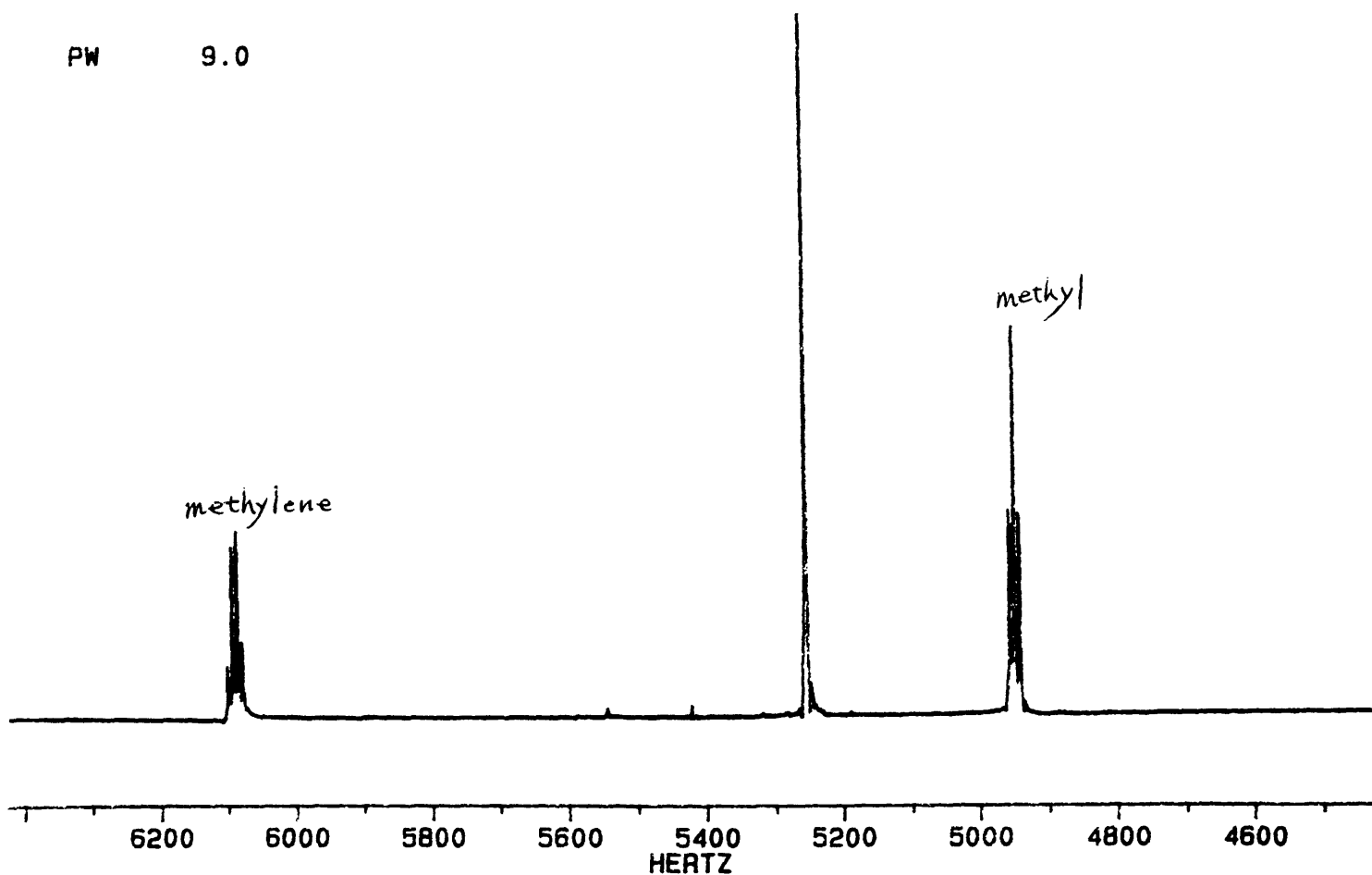
Figure 3.1 Ethyl Acetate Spectrum with no multiple quantum filtering

Chapter III

3.1 Double Quantum Filter

A. Phase Cycling

To determine the advantages and the disadvantages of the proposed method, the traditional double quantum filtering method using phase cycling was tested. Figure 3.2 shows the result of 1-D double quantum filtering using 4 phase cycling steps. Figure 3.3 shows the result of 1-D DQF with extensive phase cycling (32 cycles).

ETHYL ACETATE SPECTRUM WITH 4 PHASE CYCLING

BRUKER

EACETATE.004

PW   0.0

acetate

methylene

methyl

6200   6000   5800   5600   5400   5200   5000   4800   4600
HERTZ
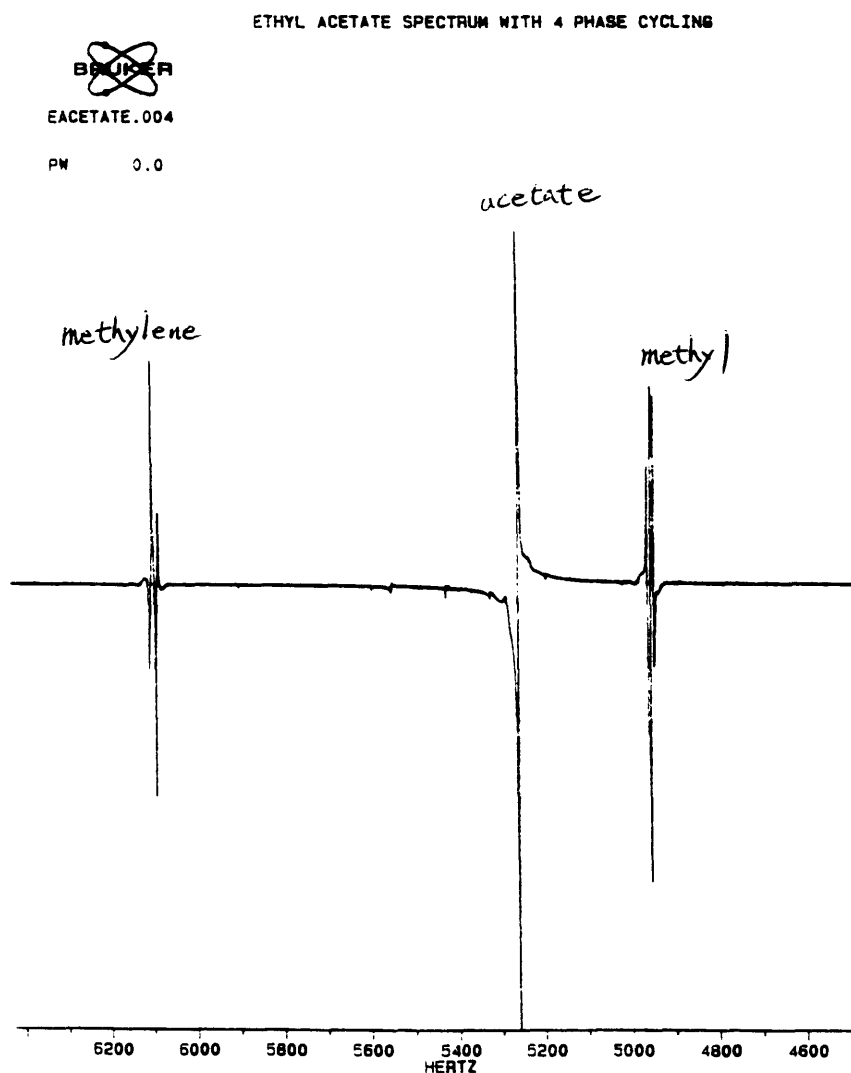
Figure 3.2 Ethyl Acetate Spectrum with 4 phase cycling steps DQF

Section 3.1

ETHYL ACETATE WITH 32 PHASE CYCLING

BRUKER

EACETATE.006

PW   0.0

methyl

methylene

acetate

6200   6000   5800   5600   5400   5200   5000   4800   4600

HERTZ
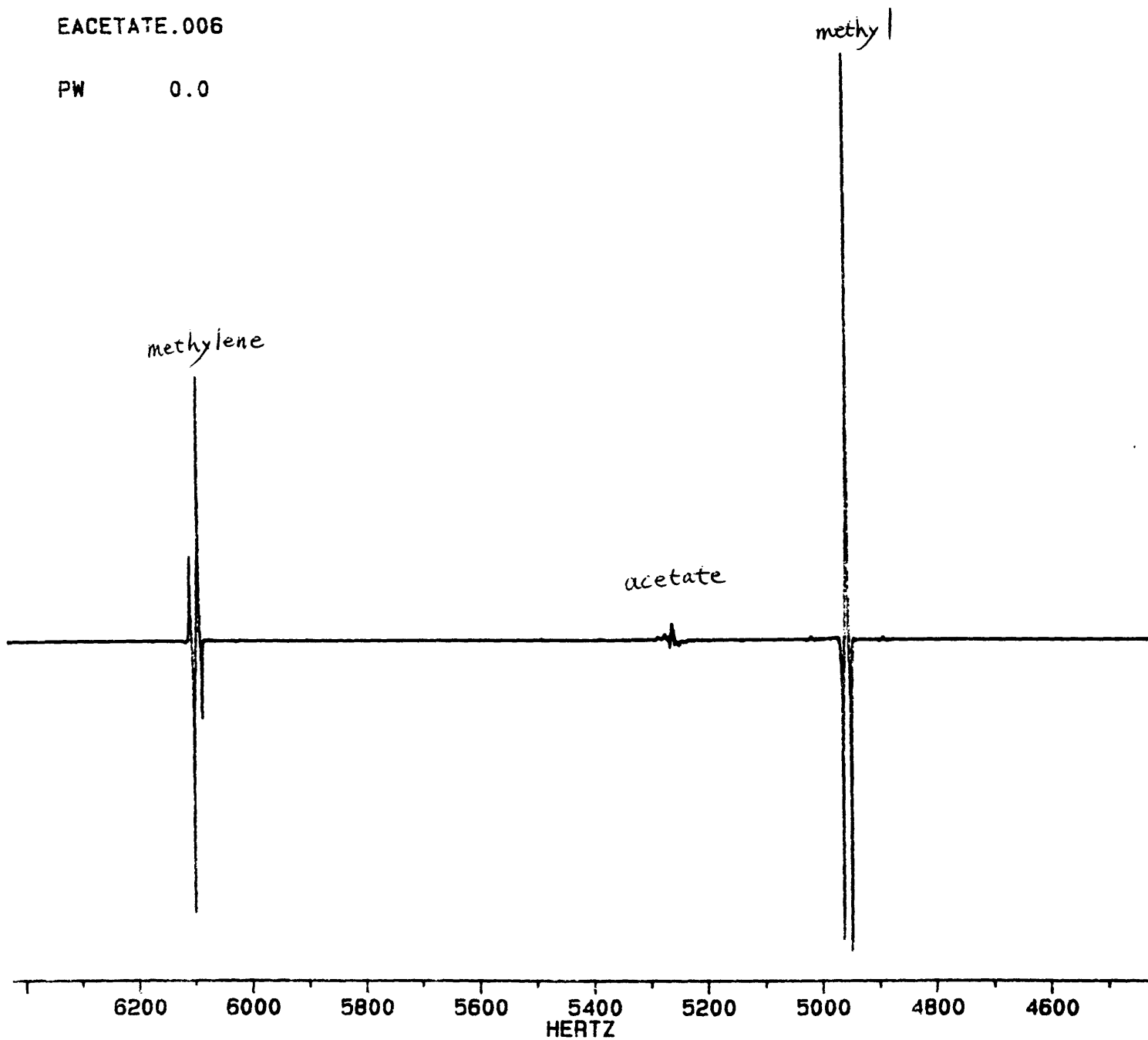
Figure 3.3 Ehtyl Acetate Spectrum with 32 phase cyling steps DQF

Section 3.1

B. RF Gradient DQF Version1

Now, we implemented the RF gradient DQF with following pulse sequence, 90x-180x-gy-2gx. Figure 3.4 shows its 1-D result.

ETHYL ACETATE SPECTRUM WITH RF GRADIENT 90X-180X-GY-2GX

EACETATE.008

PW   0.0

methylene

acetate

methyl

```
6200    6000    5800    5600    5400    5200    5000    4800    4600
                                HERTZ
```
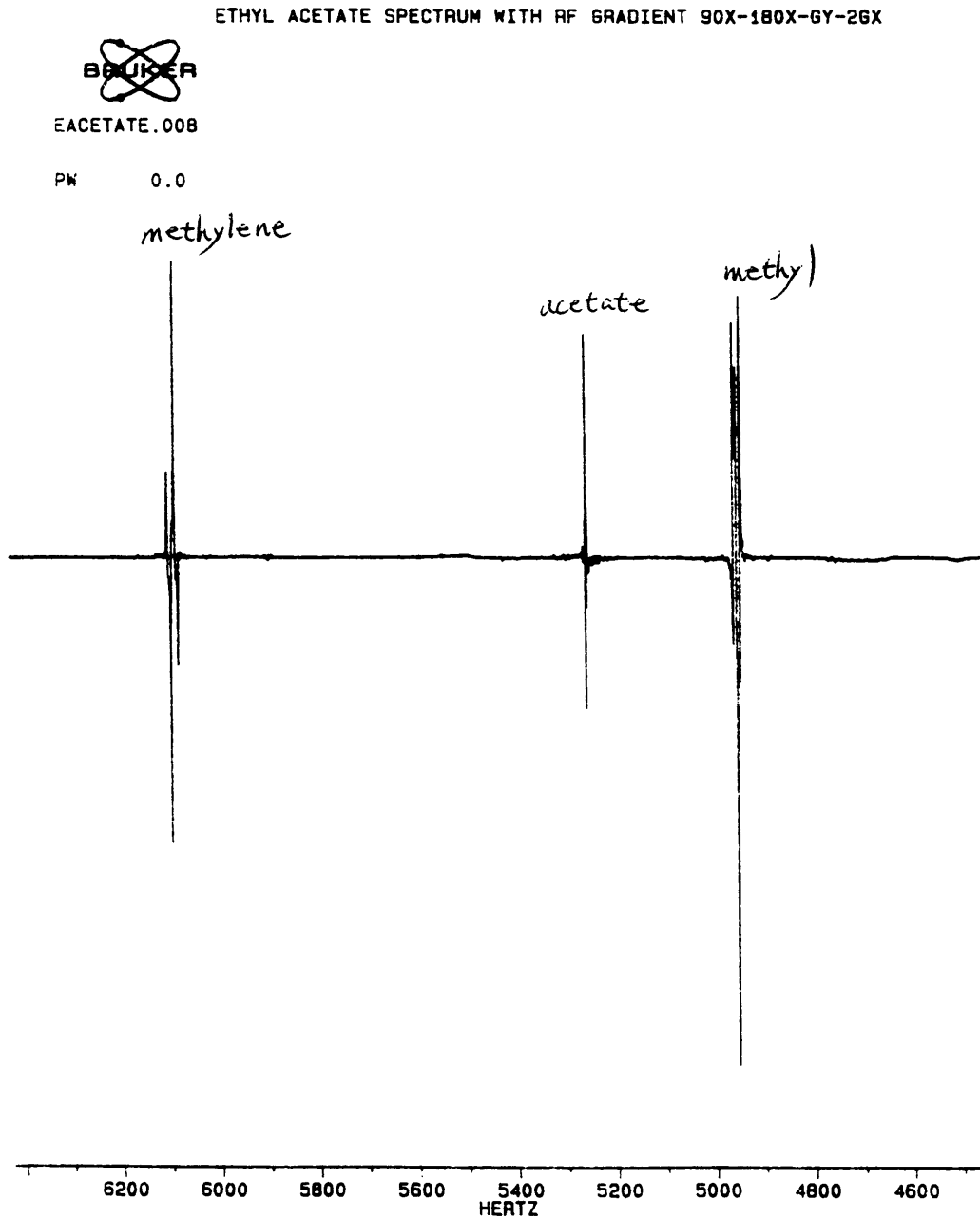
Figure 3.4. Ethyl Acetate Spectrum with RF gradient DQF version 1

Section 3.1

C. RF Gradient DQF Version 2

The following pulse sequence was implemented, 90x-1/4J-180x-1/4J-90x-gx-2gy. Figure 3.5 shows the 1-D result.

ETHYL ACETATE SPECTRUM WITH RF GRADIENT 90X-180X-90X-GX-2GY

EACETATE.012

PW   0.0

methylene   acetate   methyl

6200   6000   5800   5600   5400   5200   5000   4800   4600
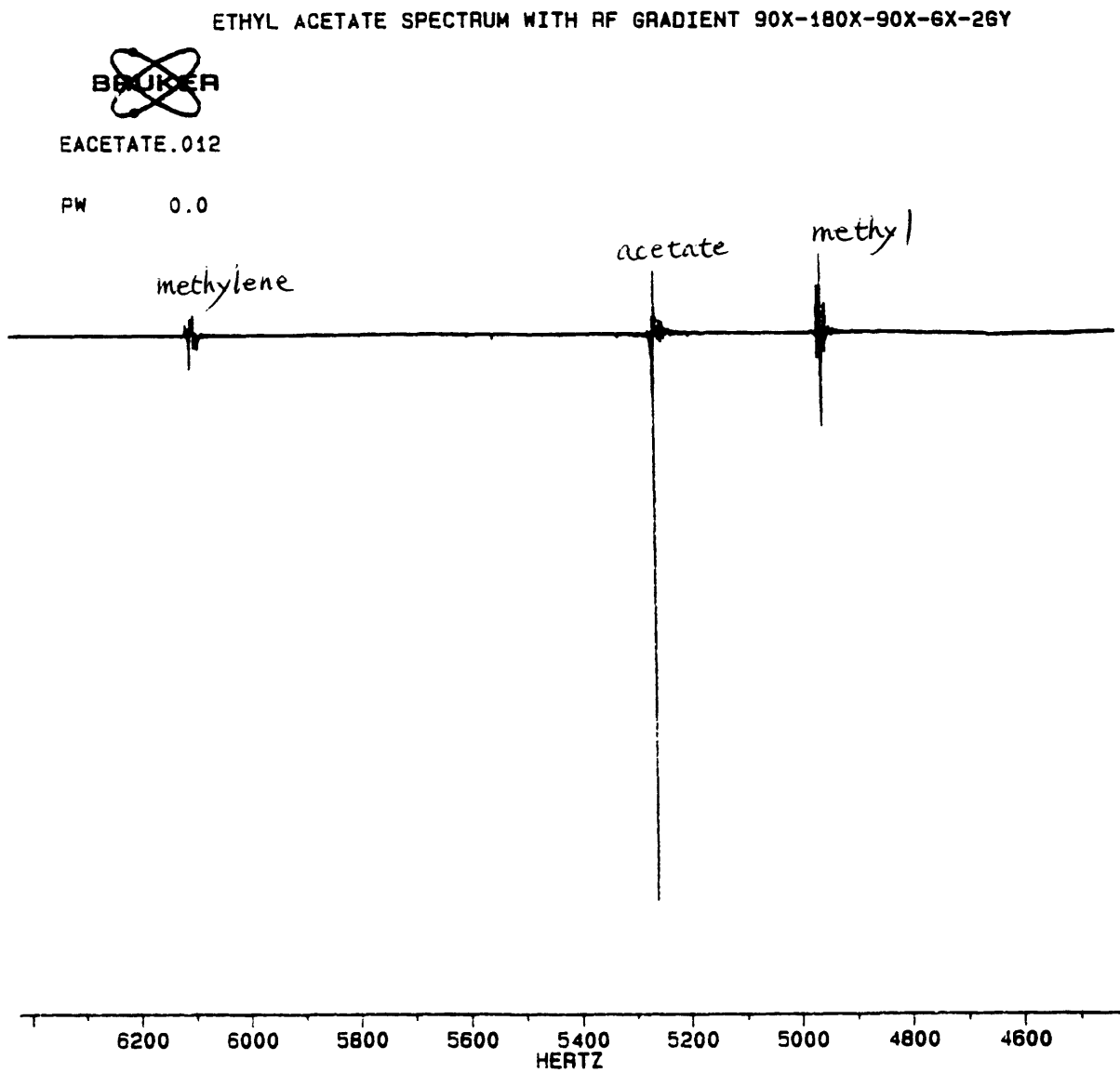HERTZ

Figure 3.5 Ethyl Acetate Spectrum with RF gradient DQF version 2

Section 3.2

D. RF Gradient DQF Version 3

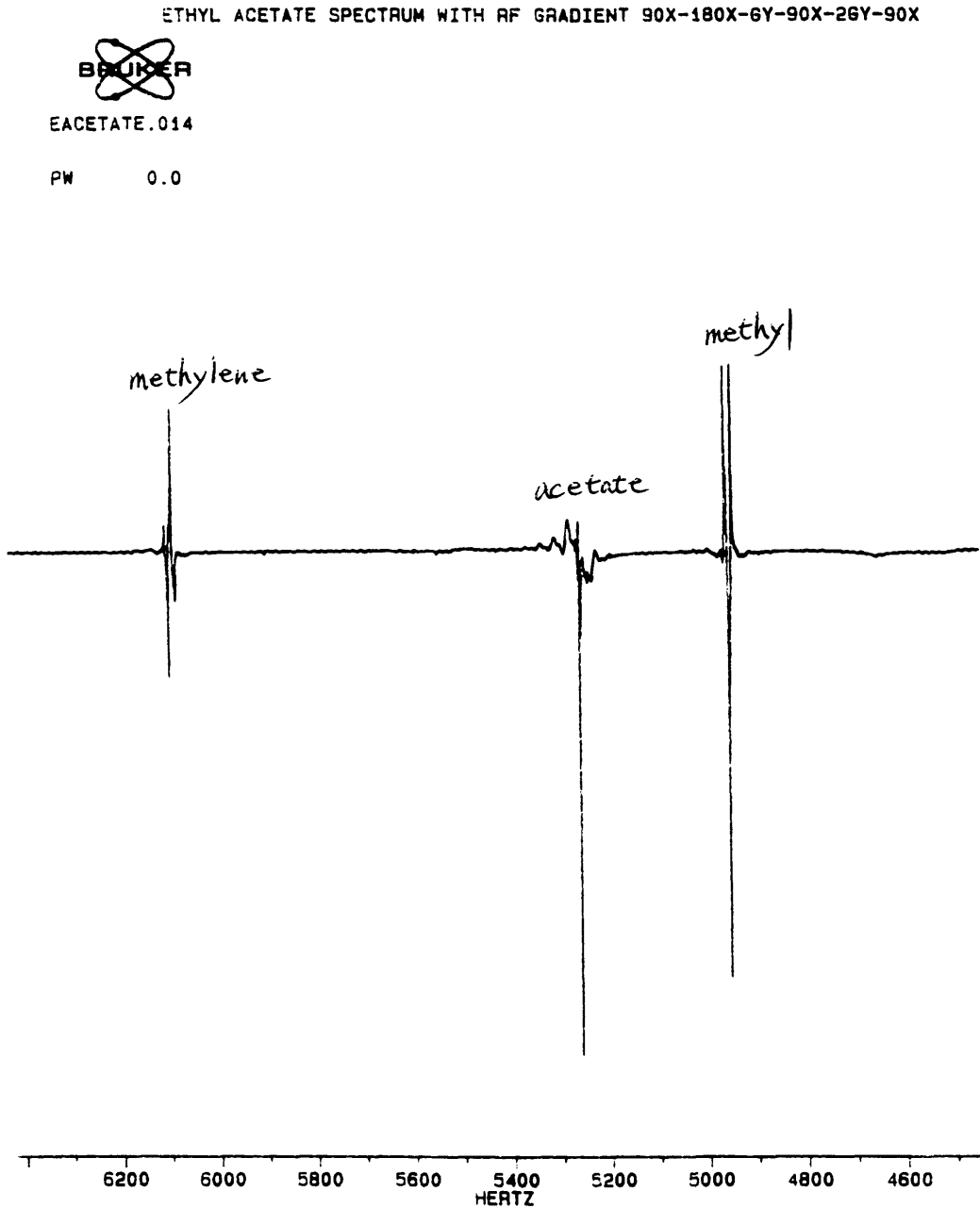Figure 3.6 shows the 1-D result of the following pulse sequence 90x-180x-gy-90x-2gy-90x.

ETHYL ACETATE SPECTRUM WITH RF GRADIENT 90X-180X-GY-90X-2GY-90X

EACETATE.014

PW   0.0

Figure 3.6 Ethyl Acetate Spectrum with RF Gradient DQF version 3

Section 3.1

3.2 Triple Quantum Filter

A. Phase Cycling

Figure 3.7 shows the result of 1-D triple quantum filtering using 48 phase cycling. The reason for using such an extensive cycling is trying to remove noise caused by the inhomogeneity of the field gradient and noises resulted from less than perfect instrumentation. Unfortunately, as can be seen from the graph, this scheme did not work out too well.

ETHYL ACETATE WITH TQF 48 PHASE CYCLING

BRUKER

EACETATE.016

PW   0.0   acetate

                    methylene   methyl

```
        6200    6000    5800    5600    5400    5200    5000    4800    4600
                                        HERTZ
```
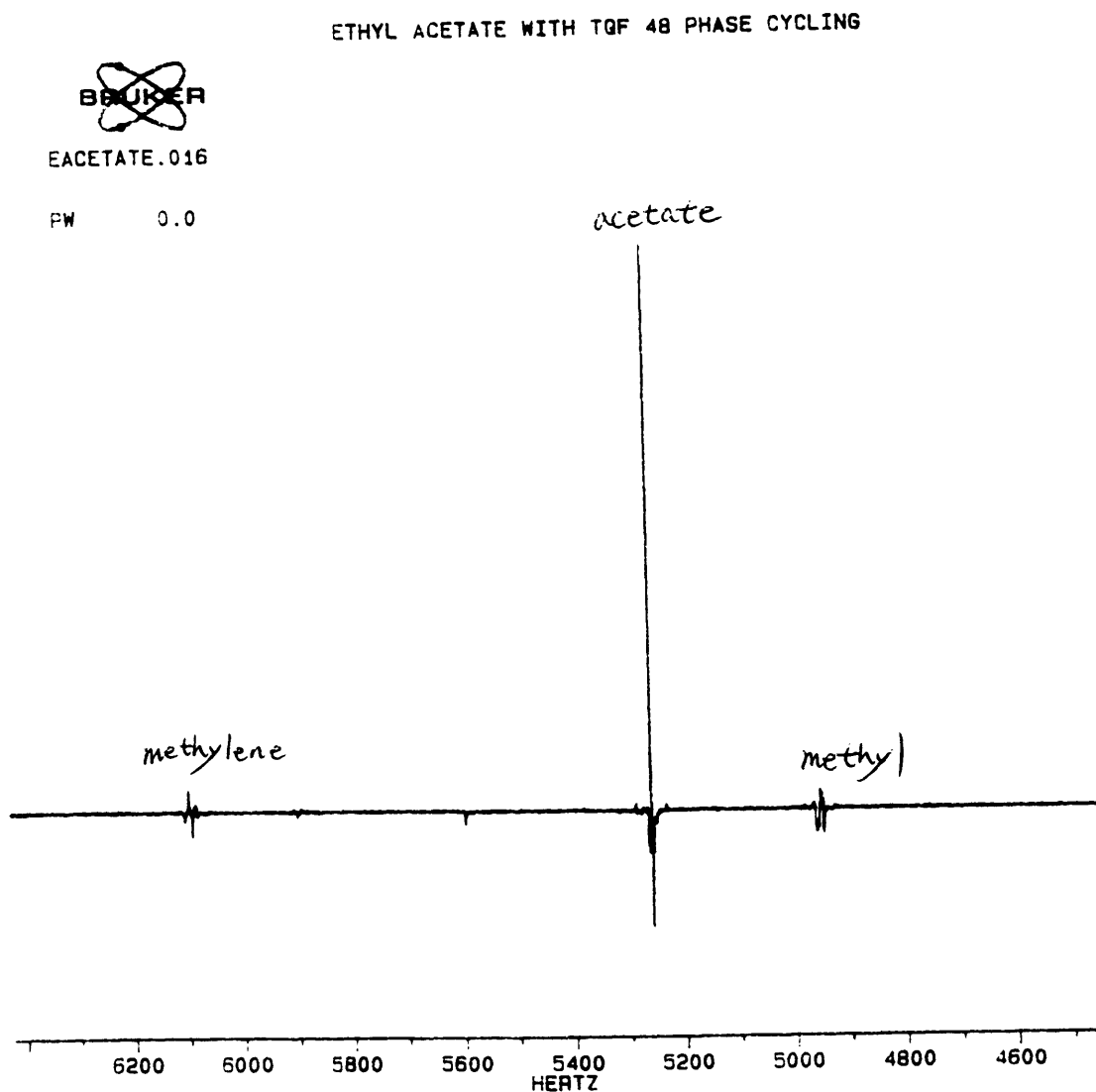
Figure 3.7 Ethyl Acetate Spectrum with extensive physe cycling TQF

Section 3.2

B. RF Gradient TQF Version 1

Figure 3.8 shows the result of 1-D triple quantum filter with the following pulse sequence 90x-180x-gx-90x-3gy-90x. The 90 degree pulses following the rf gradients are used to convert the spins into observables

ETHYL ACETATE SPECTRUM WITH RF GRADIENT 90X-180X-GX-90X-3GY-90X
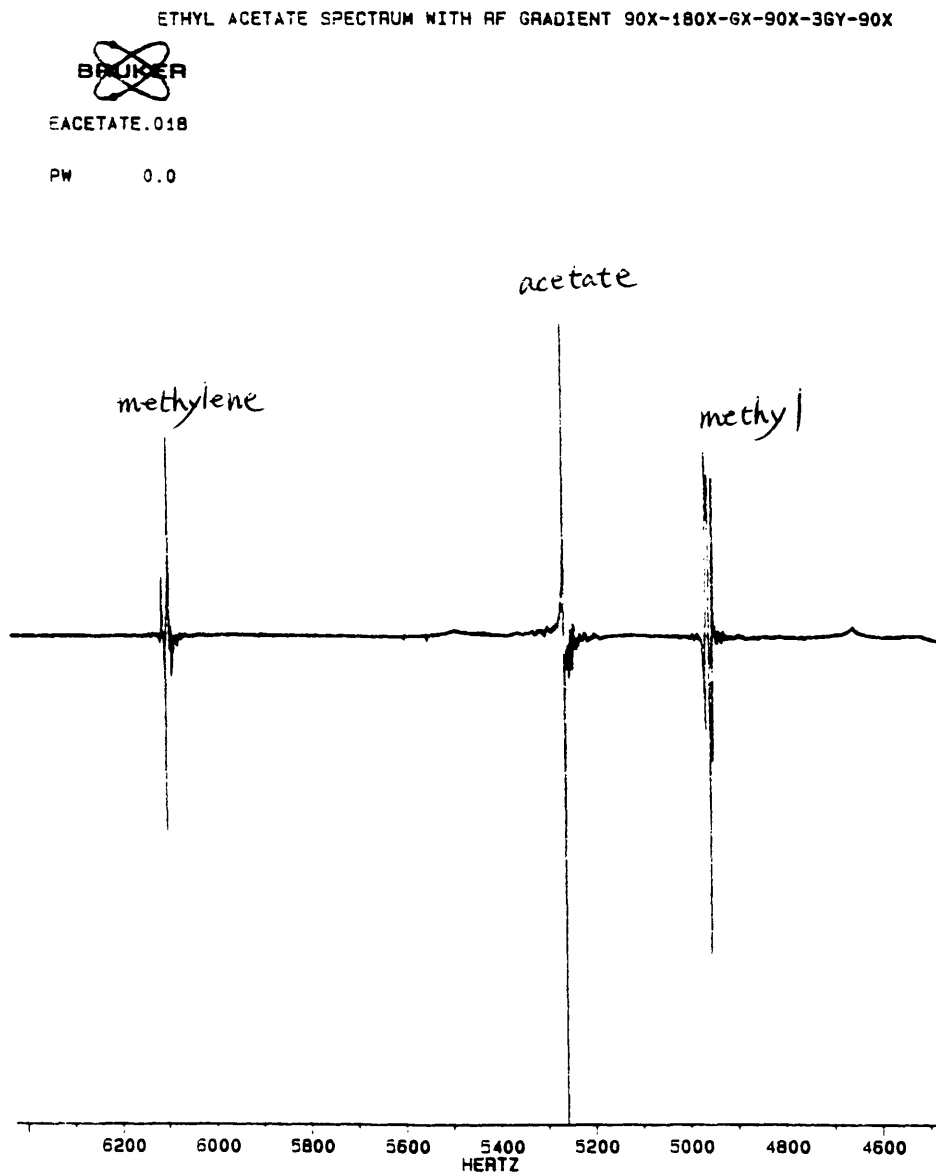
EACETATE.018

PW   0.0

Figure 3.8 Ethyl Acetate Spectrum with RF Gradient TQF version 1.

Section 3.2

C. RF Gradient TQF Version 2

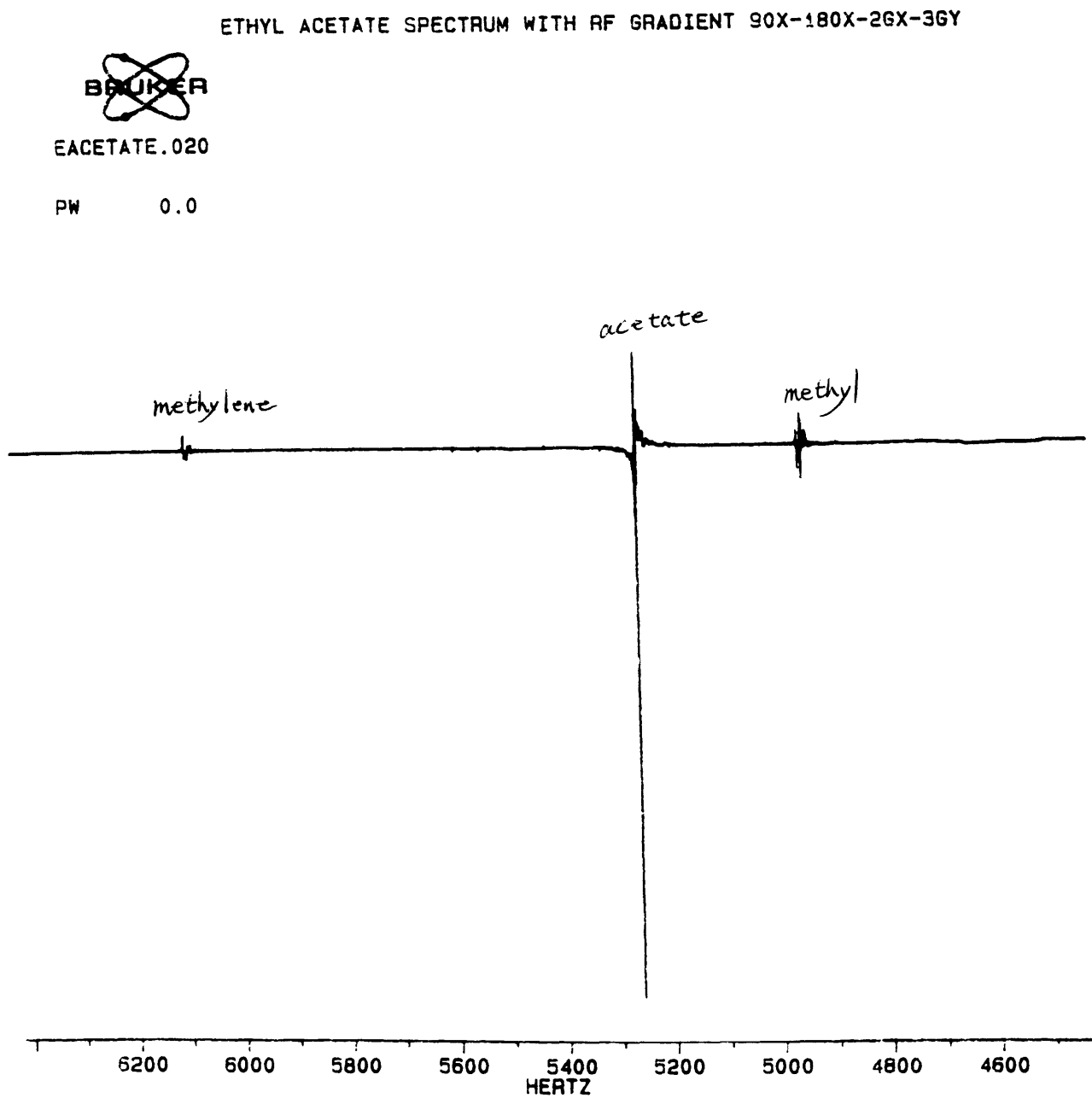Figure 3.9 shows the 1-D result of the following sequence 90x-180x-2gx-3gy.

ETHYL ACETATE SPECTRUM WITH RF GRADIENT 90X-180X-2GX-3GY

EACETATE.020

PW   0.0

Figure 3.9 Ethyl Acetate Spectrum with RF Gradient TQF version 2

Section 3.2

3.3 Quadruple Quantum Filter

A. Phase Cycling

Since the suppression effect of the triple quantum filter phase cycling was not very good, it seems that an extremely extensive cycling scheme would be needed to achieve the filtering effect for quadruple quantum filtering. Therefore, no experiment was conducted for QQF phase cycling.

B. RF Gradient QQF Version 1

Figure 3.10 shows the result of 1-D quadruple quantum filter with the following pulse sequence 90x-180x-gy-4gx-90y.
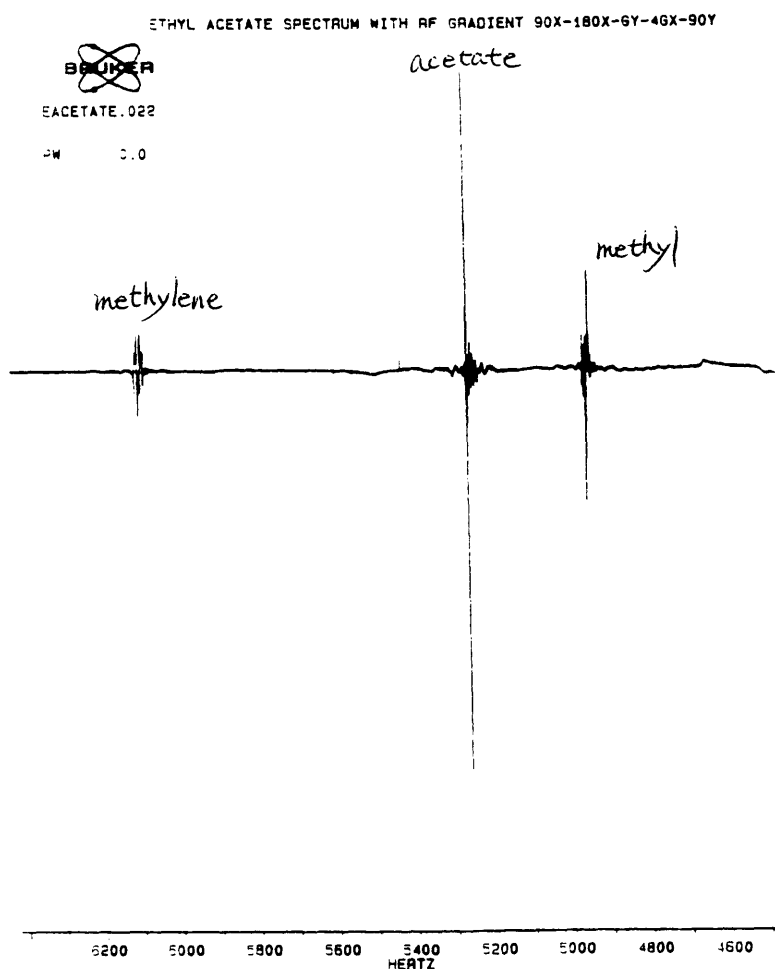

Figure 3.10 Ethyl Acetate Spectrum with RF Gradient QQF

Section 3.3

3.4 Discussion

From the plots we can clearly see that multiple quantum filtering using RF gradients can suppress the unwanted spin signals, so the unwanted signal will be of similar intensity and magnitude as signals derived from the desired coherence transfer pathways. Unfortunately, the spectra obtained from the RF gradient multiple quantum filters are not as good as they should be. Theoretically, RF gradient method should give better, if not at least as good, spectra as that obtained via phase cycling method. Our results showed that the RF gradient methods did not suppress the signal as well as the phase cycling experiments. There are several factors which might contribute to this result. First, since we used residual inhomogeneity of the Bo field as our RF gradient, the effective RF gradient is very weak. This weak RF gradient field could not dephase the spin system efficiently. This is particularly true in the presence of appreciable resonance offsets which can act to second average the RF gradient to zero. Apart from the inefficient dephasing, with small RF gradients, longer RF pulses are required for dephasing. With longer pulses, the RF amplifier and probe will heat up. This can induce changes in the impedance, which leads to the phase of RF pulses changing. This phase transient would also contribute to poor dephasing and in particular, to spin locking of the undesired coherences. Other factors which might improve the overall quality of the spectrum include better shimming of the magnet and more appropriate pulse duration.

Chapter IV

Conclusion

Multiple quantum filtering can suppress unwanted signals, such as that of the solvent, and leave only the signals from the desired quantum coherence states. By applying the multiple quantum filters, the spectrum is easier to decipher, and the internuclei conformation of the molecules may be more easily determined. Therefore, multiple quantum filtering techniques are widely used for the study of the structures of complex biomolecules. Traditionally, multiple quantum filtering is performed by phase cycling, recently, however, field gradient methods have been explored as alternatives, using either B_0 field or RF gradient. We explored multiple quantum filtering by Radio Frequency gradients.

The RF gradient method is potentially better than the phase cycling method because: 1) it takes advantage of the RF field inhomogeneity to create a spatial averaging of nutation angles in one scan, as opposed to phase cycling which requires many scans to average out the undesired coherence pathway, so the RF gradient method can decrease the time it takes to do NMR experiments; and 2) since RF gradient method suppresses the large solvent resonance signal from the beginning, it could decrease t1 noise, and increase the dynamic range of the A-to-D converter.

The RF gradient method also has advantages over B_0 field gradient method because 1) the RF gradient switching time is short; 2) it does not affect the lock channel; 3) since, RF gradient is nonsecular, so it does not commute

with internal Hamiltonians as B0 field does, so it does not introduce line broadening due to chemical shifts, therefore, no distortion of lineshape; 4) it does not induce any eddy current; and 5) the RF gradient is frequency selective, it will dephase only A or B resonance, while B_0 field will affect both A and B nuclei [10].

Chapter IV

Bibliography

[1] J. Brondeau, D. Boudot, P. Mutzenhardt, and D. Canet: The Equivalent of the DQF-COSY Experiment, with One Transient per t1 Value, by Use of B_1 Gradients. *Journal of Magnetic Resonance* 100-611-618, 1992

[2] D. Canet, P. Tekely, N. Mahieu, and D. Boudot: Averaging Effects in NMR Spectroscopy by a Radio-Frequency Field Gradient: Induced Coherence Transfers. *Chemical Physics Letters* 182: 541-545, 1991

[3] D. G. Cory, F. H. Laukien and W.E. Maas:NMR Spectroscopy with Radial Pulses. p- and n-type Selection COSY. *Chemical Physics Letters* 212:487-492, 1993

[4] D.G. Cory, F. H. Laukien, and W. E. Maas: Double-Quantum-Filtered-COSY B1-Gradient Experiments. *Journal of Magnetic Resonance, Series A* 105:223-229, 1993

[5] C. J. R. Counsell, M.H. Levitt, and R.R. Ernst: The Selection of Coherence-Transfer Pathways by Inhomogenous z Pulses. *Journal of Magnetic Resonance* 64: 470-478, 1985

[6] R. R. Ernst, G. Bodenhausen, and A. Wokaun. *Principles of Nuclear Magnetic Resonance in One and Two Dimensions.* New York, NY, Oxford University Press Inc. New York, 1987

[7] P. Güntert, M. Schaffer, G. Otting, and K. Wüthrich: POMA: A Complete Mathematica Implementation of the NMR Product-Operator Formalism. *Journal of Magnetic Resonance. Series A* 101:103-105, 1993

[8] H. Kessler, M. Gehrke, and C. Griesinger: Two-Dimensional NMR Spectroscopy: Background and Overview of the Experiments. *Angew. Chem. Int. Ed. Engl.* 27:490-536, 1988

[9] R. W. Kriwacki and T.P. Pitner: Current Aspects of Practical Two-Dimensional (2D) Nuclear Magnetic Resonance (NMR) Spectroscopy: Applications to Structure Elucidation. *Pharmaceutical Research* 6:531-554, 1989

[10] W.E. Maas, F. Laukien, and D.G. Cory: Coherence Selection by Radio-frequency Gradients. *Journal of Magnetic Resonance, Series A* 103:115-117, 1993

[11] O.W. Sorensen, G.W. Eich, M.H. Levitt, G.Bodenhausen, and R.R. Ernst: Product Operator Formalism for the Description of NMR Pulse Experiments. *Progr. NMR Spectroscopy* 16:163-192, 1983

[12] K. Wüthrich. *NMR of Proteins & Nuclei Acids.* New York, NY, John Wiley & Sons, Inc., 1986

Appendix

Spectrometer Pulse Programs

Phase Cycling Double Quantum Filter

Version 1 (DQF.AU)

; double quantum with 4 phase cycling

; 90-D2-180-D2-90-D3-90-FID

1 ZE

2 D1

3 P1

4 D2

5 P2

6 D2

7 P1

8 D3

9 P1 PH1

10 GO=2 PH2

11 EXIT

PH1=0 1 2 3

PH2=R0 R2 R0 R2

; P1=90 degree, P2=180 degree

; D1=3 sec, D2=1/4J=35 msec for ^{1}H, D3=5 usec

; NS=4*N

Version 2 (DQFPH.AU)

; double quantum with extensive phase cycling
; 90-D2-180-D2-90-D3-90-FID
1 ZE
2 D1
3 P1 PH1
4 D2
5 P2 PH2
6 D2
7 P1 PH1
8 D3
9 P1 PH3
10 GO=2 PH4
11 EXIT

PH1=0 2 1 3 1 3 2 0
PH2=0 2 1 3 1 3 2 0
      0 2 1 3 1 3 2 0
      2 0 3 1 3 1 0 2
      2 0 3 1 3 1 0 2
PH3=0 0 0 0 1 1 1 1
      2 2 2 2 3 3 3 3
PH4=R0 R0 R2 R2 R1 R1 R3 R3
      R2 R2 R0 R0 R3 R3 R1 R1
; P1=90 degree, P2=180 degree
; D1=3 sec, D2=1/4J=15 msec, D3=3 usec

RF Gradient Double Quantum Filter

Version 1 (DQFRF.AU)

; DQF-RF-1D

; 90x-1/4J-180x-1/4J-Gy-2Gx

1 ZE

2 D1

3 P1 PH1

4 D2

5 P2 PH1

6 D2

7 P5 PH2

  D3

8 P7 PH3

9 GO=2 PH4

  EXIT

PH1=0

PH2=1

PH3=0

PH4=R1

; P1=90 degree, P2=180 degree, P5=600 usec, P7=1200 usec

; D1=3 sec, D2=15 msec, D3=3 usec

RF Gradient Double Quantum Filter

Version 2 (DQFD.AU)

; 90y-1/4J-180y-1/4J-Gx-2Gy

1 ZE

2 D1

3 P1 PH2

4 D2

5 P2 PH2

6 D2

7 P5 PH1

8 P7 PH2

9 GO=2

  EXIT

PH1=0

PH2=1

; P1=90 degree, P2=180 degree, P5=600 usec, P7=1200 usec

; D1=3 sec, D2=35 msec

; P1=9 usec, P2=18 usec

Version 3 (DQFE.AU)

; 90x-1/4J-180x-1/4J-90x-3usec-Gx-2Gy

1 ZE

2 D1

3 P1 PH1

4 D2

5 P2 PH1

6 D2

7 P1 PH1

8 D3

9 P5 PH1

  D3

10 P7 PH2

11 GO=2 PH3

  EXIT

PH1=0

PH2=1

PH3=R0

; P1=90 degree, P2=180 degree, P5=600 usec, P7=1200 usec

; D1=3 sec, D2=15 msec, D3=3 usec

Version 4 (DQFF.AU)

; 90x-1/4J-180x-1/4J-Gy-90x-2Gy-90x

1 ZE

2 D1

3 P1 PH1

4 D2

5 P2 PH1

6 D2

7 P5 PH2

8 P1 PH1

9 P7 PH2

10 P1 PH1

11 GO=2 PH3

  EXIT

PH1=0

PH2=1

PH3=R1

; P1=90 degree, P2=180 degree, P5=600 usec, P7=1200 usec

; D1=3 sec, D2=35 msec

; P1=9 usec, P2=18 usec

Phase Cycling Triple Quantum Filter (TQF1DPH.AU)

; 3 quantum (TQF)-1D

; 90-D2-180-D2-90-D3-90-FID

1 ZE

2 D1

3 P1 PH1

4 D2

5 P2 PH1

6 D2

7 P1 PH2

8 D3

9 P1 PH3

10 GO=2 PH4

   EXIT

PH1=(12) 0 2 4 6 8 10 0 2 4 6 8 10

         3 5 7 9 11 1 3 5 7 9 11 1

         6 8 10 0 2 4 6 8 10 0 2 4

         9 11 1 3 5 7 9 11 1 3 5 7

PH2=(12) 0 2 4 6 8 10 3 5 7 9 11 1

         3 5 7 9 11 1 6 8 10 0 2 4

         6 8 10 0 2 4 9 11 1 3 5 7

         9 11 1 3 5 7 0 2 4 6 8 10

PH3=(12) 0 0 0 0 0 0 3 3 3 3 3 3

         3 3 3 3 3 3 6 6 6 6 6 6

         6 6 6 6 6 6 9 9 9 9 9 9

         9 9 9 9 9 9 0 0 0 0 0 0

PH4=R0 R2 R0 R2 R0 R2 R2 R0 R2 R0 R2 R0

     R1 R3 R1 R3 R1 R3 R3 R1 R3 R1 R3 R1

     R2 R0 R2 R0 R2 R0 R0 R2 R0 R2 R0 R2

     R3 R1 R3 R1 R3 R1 R1 R3 R1 R3 R1 R3

; P1=90 degree, P2=180 degree

; D1=10 sec, D2=15 msec, D3=3 usec

;NS=6*N

RF Gradient Triple Quantum Filter

Version 1 (TQFRF.AU)

```
; 3 quantum (TQF)-1D
; 90x-1/4J-180x-1/4J-Gx-90x-3Gy--90x-FID
1 ZE
2 D1
3 P1 PH1
4 D2
5 P2 PH1
6 D2
7 P4 PH1
  D3
8 P1 PH1
  D3
9 P7 PH2
  D3
10 P1 PH1
11 GO=2 PH3
12 EXIT

PH1=0
PH2=1
PH3=R0
; P7=3*P4
; P1=90 degree, P2=180 degree, P4=400 usec, P7=1200 usec
; D1=3 sec, D2=15 msec, D3=3 usec
```

Version 2 (TQFRF2.AU)

```
; 3 quantum (TQF)-1D
; 90x-D2-180x-D2-2Gx-3Gy-FID
1 ZE
2 D1
3 P1 PH1
4 D2
5 P2 PH1
6 D2
7 P6 PH1
  D3
8 P7 PH2
9 GO=2 PH3
  EXIT

PH1=0
PH2=1
PH3=R0
; P1=90 degree, P2=180 degree, P6=800 usec, P7=1200 usec
; D1=3 sec, D2=35 msec, D3=3 usec
```

RF Gradient Quadruple Quantum Filter

; 4 quantum (QQF)-1D
; 90x-D2-180x-D2-Gy-4Gx-90y
1 ZE
2 D1
3 P1 PH1
4 D2
5 P2 PH1
6 D2
7 P3 PH2
  D3
8 P7 PH1
  D3
9 P1 PH2
10 GO=2 PH3
11 EXIT

PH1=0
PH2=1
PH3=R1
; P1=90 degree, P2=180 degree, P3=300 usec, P7=1200 usec
; D1=3 sec, D2=15 msec, D3=3 usec